FRACTURE MECHANICS FOR RAIL CRACK FORMATION

DESIGN OF A NUMERICAL MODEL TO PREDICT ROLLING CONTACT FATIGUE ON RAILS

K. SLAGTER

UNIVERSITY OF TWENTE,
ENGINEERING TECHNOLOGY

25.10.2024

Summary

Train rails are highly susceptible to surface damage and surface defects such as wear and rolling contact fatigue (RCF). Because of this damage, it is of great importance to maintain rails before critical defects arise. The Whole Life Rail Model (WLRM) is a model that could be used as a tool to predict maintenance needs for rails. In this model, the wear number is used as an indicator to predict the number of cycles a train can run over the rail before critical damage arises. This wear number is based on the shear forces exerted by the train wheel and the creepage, the relative velocity between the wheel and the rail. The vertical axis of the WLRM shows the Damage Index, the inverse of the number of cycles until critical damage.

Because the existing WLRM is completely built upon field results at specific locations, it is not possible to use it for all locations and cases. In this study, it is tried to design an approach that can describe the RCF function of the WLRM. Together with already existing wear models, WLRMs can be developed for each location.

To construct this approach, the fatigue crack formation is divided into crack initiation and crack propagation. In this study, the focus was mainly on propagation. An XFEM model was used to determine the Stress Intensity Factors (SIFs) in a crack tip, when a train wheel is crossing the rail. These SIFs could be used to obtain the crack growth rate. By using a critical crack length of 10 mm, the number of cycles until critical crack length, and thus the Damage Index could be determined.

The obtained Damage Indices were used to reconstruct the RCF curve of the existing WLRM. It was found that operational parameters have an important contribution to the determination of the wear number and Damage Index. By keeping these parameters close to the values from the field locations, the existing RCF curve could be reconstructed.

As these operational parameters proved to be influential, it was analysed how these different parameters influence the formation of the RCF function. For this, the vertical wear depth, curve radius, rail cant, friction coefficient, train speed, longitudinal suspension stiffness, lateral suspension stiffness and axle load were used, as these have proven to be important parameters for wear. The size of these parameters was varied such that the change in Damage Index and wear number could be obtained. For parameters such as the load, speed and curvature, significant changes in either wear number or Damage Index were found. On the other hand, both stiffnesses proved to be of little significance.

After showing the influence of different parameters, a regression formula was set up and trained. Using this formula, it became possible to estimate the Damage Index if the values for the eight mentioned parameters are known. The Damage Indices found by the XFEM model were compared with the ones found by the formula. In this way, it was shown that the formula is able to predict Damage Indices with less than 10 % error. Using this formula, the Damage Index was plotted against the size of the operational parameter. These plots generally showed comparable results to the earlier performed analysis on these parameters. It was shown that most parameters have a strong linear relation with the Damage Index. For some parameters, the rail cant and the axle load, the curve is not totally straight and thus, also some quadratic influence is expected. The vertical wear depth showed parabolic behaviour. This parameter showed to be more difficult to explain, higher order terms could be involved for the wear depth.

Using the XFEM model, it was tried if to analyse a theoretical case where a rail was simulated with a fixed wear depth, radius and cant. It was assumed that multiple different trains would make use of the rail, and thus the axle load, stiffnesses, speed and coefficient of friction were varied. For multiple of these situations, Damage Indices and wear numbers were obtained. These results did not form a straight line and thus the construction of an RCF function was not possible. As the parameter influence is the cause for this, it is not expected that other cases where multiple parameters are varied do form a straight RCF curve.

To be able to use the propagation model to predict the Damage Index, it was proposed to determine the Damage Index for wear and for RCF. Both can be determined using their own prediction model. By comparing both Indices with each other, it can be determined which failure is most dominant and if it necessary to take the other failure mechanism into account. This method could be used to give an indication of the important failure mechanism and the number of cycles before critical damage.

It has not been possible to construct the WLRM for different situations in this study. Some important parts of the model are still missing to get a full view of the crack growth in rails. The initiation phase is still missing, and will increase the number of cycles until critical damage when it is included. In the propagation model, the crack growth rate is kept at a constant rate. As this rate can change depending on the geometry of the crack (which will change when the crack grows), changing growth rate should also be included in some way in the prediction model.

Although construction of the WLRM was not possible, it has been shown that crack propagation in rails can be predicted and used to predict the number of cycles until critical damage.

Contents

List of Figures

List of Tables

1 | Introduction

Railway traffic, passenger trains as well as freight trains, have significantly increased over the years. This, as well as the introduction of new trains, new materials for wheels and rails, has led to higher maintenance costs and downtime. Rail surface defects cause a large part of these costs and downtime. Rail surface defects are caused by a combination of wear and Rolling Contact Fatigue (RCF). One of the most occurring RCF defect types is head checks, surface defects formed on top of the rail. If these are not removed in time, they will grow to fatal crack sizes and eventually lead to broken rails. To prevent this from happening, the currently existing corrective and preventive maintenance strategies should be adjusted. The chosen strategy should be more based on predictive approaches, as this will help to forecast certain defects on the rail. By using predictive maintenance strategies, the degradation of the track can be estimated and the length of maintenance intervals can be based on this. To be able to predict the degradation of the rails, models have been developed which predict the damage rate due to RCF and wear. The Whole Life Rail Model (WLRM) is one of these models and can predict the damage rate based on the relative wear on the rails. The drawback of this model however is that it is based on field data from some specific locations with specific properties. Therefore, the WLRM as set up by Burstow [1] is not representative for different scenarios and cannot be used for other pieces of railway track.

Because of this, a generic framework will be developed during this study. This framework should make it possible to construct a WLRM for most of the possible scenarios. As the WLRM is based on an RCF model and a wear model, both should be determined to be able to construct a complete WLRM. In this thesis, the focus will be on the RCF model and its accompanying damage function. The wear function and associated wear rates have already been derived by Meghoe [2] from analytical expressions of several physics-based models. The RCF part of the WLRM however still has to be derived, preferably by a nonlinear fracture mechanics approach. Therefore, this research will analyse different models available to describe RCF damage and use one of these to reconstruct the RCF part of the WLRM. This chapter will further describe the background of the study, the research problem, the aim, objective, research questions, and the research hypothesis.

1.1 Background

As discussed before, the combination of wear and RCF can cause severe problems for railway safety. RCF on railway tracks is known to cause multiple types of defects, from which head checks are one of the most common and severe, but also best-known defects of surface-initiated RCF. A visual example of these head checks is shown in Figure 1.1 [3]. Head checks commonly occur on curved tracks with radii less than 3000 m and in switches and crossings, because lateral contact forces and relative spin are generally high at these locations. They are primarily located around the gauge corner of the outer rail and are mostly found with multiple cracks together clustered at equal distances from each other. These cracks will initiate by forming short cracks at a shallow angle with the rail surface. When the crack grows, these angles can become steeper. These cracks grow to a length of approximately 30 mm after which the probability of failure becomes very high [3]. In this research, the focus will be on the initiation and propagation of these head checks.

(a) *severe Head Checks on rail surface*

(b) *Head checks in gauge corner of high rail. Traffic in x-direction*
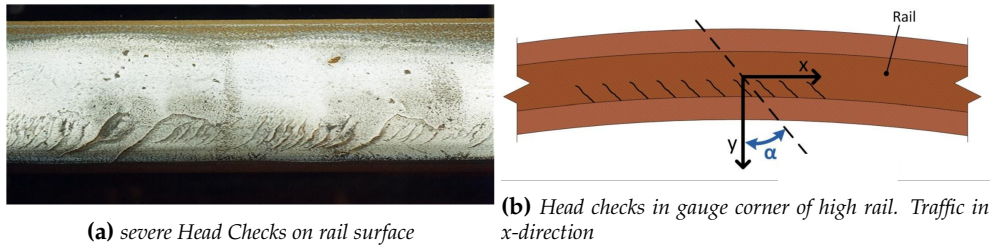
Figure 1.1: *Examples of head checks [3].*

Because head checks can cause severe problems, prediction models should be used to understand and predict when damage occurs on the tracks and to forecast when maintenance needs to be performed. As mentioned in the introduction, one of these models to predict damage is the Whole Life Rail model (WLRM), developed by Burstow [1, 4]. The WLRM is a damage function set up to predict the damage of a rail. For a specific rail material and coefficient of friction, the WLRM is depicted in Figure 1.2. The Damage Index depends on the wear number, $T\gamma$ which can be calculated for specific wheel-rail contact as;

$$T\gamma = T_x\gamma_x + T_y\gamma_y \tag{1.1}$$

In this T_x and T_y represent the tangential or shear forces, γ_x and γ_y represent the longitudinal and lateral creepage. This creepage is known as a dimensionless quantity describing the relative velocity of the train wheel moving over the rail, normalised by the rolling velocity. The x-axis is aligned with the track, and the y-axis is perpendicular to the track. It should be noted that this equation does not take into account spin creepage in the wear number, which can play a significant role in the formation of head checks. In a guide to calculate $T\gamma$ values, Burstow however writes that inclusion of spin creepage in the equation is possible and done for some cases [5].
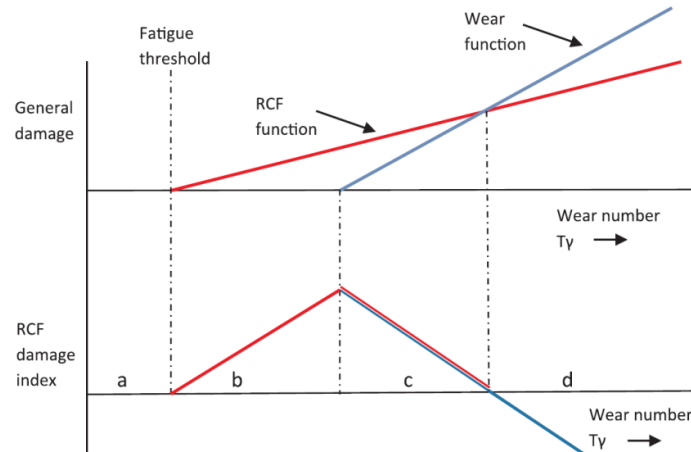
Figure 1.2: *Wear and RCF as competing mechanisms of rail surface degradation [6]*

The WLRM is based on the influence of Rolling Contact Fatigue (RCF) and wear on the rail. Therefore, the WLRM is determined with individual wear and RCF functions. In Figure 1.2 the combination of these models can be seen. In the WLRM in Figure 1.2 a clear distinction can be made between the regions a, b, c and d. In Region a, fatigue nor wear has a serious impact. This is followed by region b, where fatigue is dominant. A fatigue threshold is reached such that this mechanism becomes

important. Once this threshold is reached, the crack growth becomes detectable. Fatigue cracks are formed and the wear is not high enough to remove the layers with these cracks off the track. In region c fatigue crack initiation still happens, but wear removes (part of) these defects. Finally, in region d, wear is so dominant that fatigue cracks have no time to form or grow, the track however wears heavily.

By using the WLRM, for a certain contact condition with a value for $T\gamma$, the Damage Index for that contact condition can be found. Based on that, the number of cycles to failure can be determined. The total damage of the rail track can be calculated by the summation of the damage done by the different contact conditions, as is given in the Palmgren-miner rule:

$$D = \sum_{i=1}^{k} D_i \tag{1.2}$$

with

$$D_i = \frac{n_i}{N_i} \tag{1.3}$$

In this equation it is stated that there are k different scenarios (contact conditions) and the Damage Index value D_i for each scenario is the ratio between the number of cycles n_i with contact condition k and the number of cycles to failure N_i for that condition. The specific contact condition is represented by wear number $T\gamma$ which is plotted on the horizontal axis in the WLRM. In the end, failure happens if the accumulated damage index D reaches a value of 1.

As mentioned before, in this study, the RCF function of the WLRM will be researched. Region b in the WLRM is the most important for this. The fatigue part of the model is of interest as there are different ways to represent RCF and the crack formation and growth on rails. A model has to be found that is relatively easy to use while giving accurate results. In the WLRM, the fatigue life is described as the number of cycles as a function of the wear number. It is assumed that the fatigue life N_f can be described by the sum of the crack initiation life N_{in} and the crack propagation life N_{prop} [7]:

$$N_f = N_{in} + N_{prop} \tag{1.4}$$

By using this equation, the distinction between crack initiation and crack propagation becomes evident. To be able to predict the lifetime of a rail with sufficient detail, models for both of these stages should be found. This means that either one model should be used that can describe N_{in} as well as N_{prop} or multiple models have to be used to describe both instances separately.

1.2 Research problem

The WLRM is based on empirical results and established by using field observations from a total of six different sites over a time period of approximately two years. With these results, Burstow [1, 4] developed the WLRM for locations with similar conditions, and with identical steel grade (R220). Hiensch and Steenbergen [6] performed similar research, setting up the WLRM for steel grades R260Mn and premium R370CrHT, by using field observations on different sites. For these cases studied by Burstow, Hiensch and Steenbergen, WLRMs are thus identified. The difficulty is that for other locations, steel grades, roughness and other parameters, such as rail radii, cant, train types and weather conditions are different. Because of this, a new WLRM should be developed for each location. As data gathering from field observation is a time-consuming business, it can be seen as a major disadvantage for using the WLRM. Next to this, in the analyses of Burstow, Hiensch and Steenbergen [1, 4, 6], the coefficient of friction was set to be constant. It is however known

that parameters such as the friction coefficient have a significant influence on fatigue life [8], while they can also vary significantly. In order to improve the WLRM, the coefficient of friction, but also other parameters, such as rail radii, axle loading and train speed, should be considered. Their effects on the damage function when these parameters change have to be analysed. Important for these analysed parameters is that they are easily retractable from operational data by the end user, the asset owner. That is why more complex variables such as material properties are not analysed. Because of these reasons, it would be beneficial to be able to construct the WLRM using analytical expressions and numerical models. If this is possible, the time needed to construct a WLRM could be reduced and changing parameters such as the coefficient of friction could more easily be included in the calculations.

Once it becomes possible to numerically describe the WLRM, it also becomes possible to develop WLRMs for different situations, wheel-rail configurations, steel grades and rail dimensions. It would thus become more easy to describe the WLRM for virtually every piece of track in all situations. An advancement like this will lead to easier maintenance as it would become possible to predict maintenance needs for all possible rail tracks. As this improvement will facilitate railway maintenance, this is the main reason to perform this research.

1.3   Research aim, objectives and questions

1.3.1   Research aim

In the current knowledge, there is a theoretical gap between the experimental results from which the WLRM is constructed and a sufficiently detailed analytical model able to describe such WLRMs. As the wear model has been derived before, this study aims to develop and implement a model which is able to describe crack initiation and propagation using fracture mechanics. In the end, the aim of the research is to be able to construct a WLRM using the developed RCF damage function.

1.3.2   Research question

To get a better view of the importance of this study and the main reason why this study is performed, the following main research question is set:

How can the RCF part of the Whole Life Rail Model be reconstructed using a nonlinear local Rolling Contact Fatigue approach?

To answer this question, the research question was split up into multiple sub-questions:

- Which models are available for predicting and modelling rail crack initiation?

- Which models are available for predicting and modelling rail crack propagation?

- Which crack initiation model and which crack propagation model can best be used for reconstructing the WLRM?

- How can the RCF damage function be constructed using the selected initiation and propagation model?

- Which input parameters are most influential for the RCF damage function?

1.3.3   Approach

To perform this study in an organised manner, a strategic approach has been developed. The result of this thesis depends on being able to describe the results from the experimental field data using analytical and numerical models for crack initiation and propagation. In the end, this study aims to reconstruct the WLRM using only analytical and numerical models. The end goal is to come up with a function that can describe the damage of the rail based on rolling contact fatigue. To come to this result, a top-down approach is taken. To begin at the top, a literature review is performed to get acquainted with crack formation on rails. The general mechanics behind cracks formed by RCF should be known, such that the cause of the problem is clear. This will be followed by literature review to accomplish the first research objectives. Different models that are able to describe the formation of head checks on railway tracks will be reviewed during this step. In this review, a distinction will be made between crack initiation models and crack propagation models. Because head checks form primarily at the surface [3], special attention is being laid on models describing surface-initiated cracks.

Once suitable models are found, these are compared and the best ones are chosen to research more in-depth. To choose which models will be used, literature will be used to see which are most commonly used for rail damage purposes. The chosen models should be able to predict fatigue life and thus the output should be in fatigue life (number of cycles to failure). Next to that, the chosen models should have the right level of detail such that they can evaluate changing parameters in the RCF models with precision.

The first step with these chosen models will be to check if they can describe rail fatigue similarly as observed by Burstow [1]. Data from existing VI-Rail simulations will be compared to the field data obtained by Burstow, in order to get similar simulation values. If similar damage values and a comparable RCF function can be found using the model, further steps can be taken involving different parameters. Using VI-Rail, simulations with different variable parameters such as steel grades, surface roughness and, maybe most importantly, coefficient of friction, will be performed. The outputs from these simulations will be used in Abaqus where crack growth is simulated and stresses are measured using a FEM analysis. Using these new simulations, it is expected that an RCF function can be set up. If this function can be found, it will show the effects of the changing parameters on the fatigue life of the railway track. By finding this, the fifth objective can be accomplished. Eventually, the damage function should be integrated into the WLRM with the existing wear damage function. The end goal is reached if a function can be found that can describe RCF damage for different parameters, and can fit into the WLRM, such that damage by wear also can be considered. In Figure 1.3, a schematic overview of the different steps and chapters for this thesis is shown.
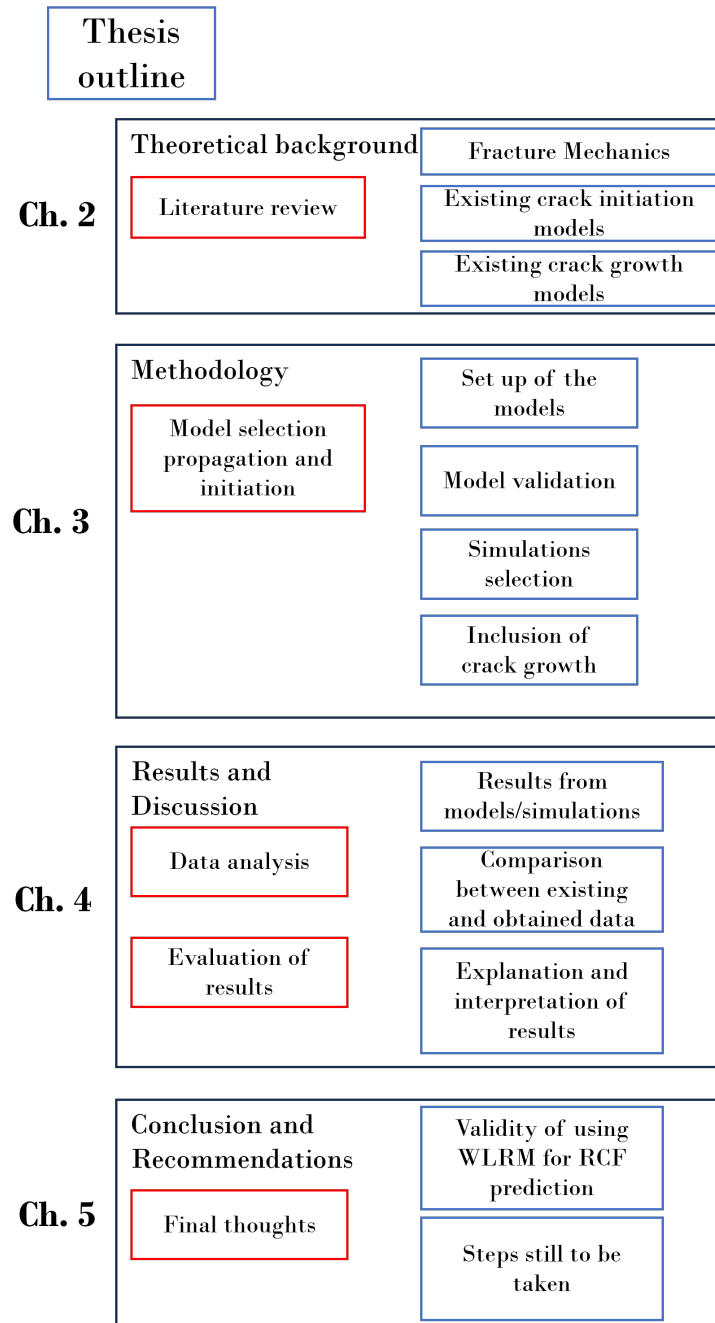
Figure 1.3: *Outline of the thesis with chapters.*

2 | Theoretical Framework

In this chapter, the theory behind crack initiation and propagation will be discussed. First, the theory behind crack formation will be explained. The difference between initiation and propagation will be discussed and the boundary between these phases will be explained. This will be followed up by explaining Fracture mechanics. A basic understanding of the mechanisms involved in crack formation will be formed. The differences between Linear Elastic Fracture Mechanics (LEFM) and Elastic Plastic Fracture Mechanics (EPFM) are laid out. Once this theory is clear, an overview of different possible models for crack initiation and propagation will be given. The aim of creating this overview is to find suitable models which can be used to predict the lifetime of rails based on fatigue life.

2.1 Crack formation

A fatigue crack is not simply formed. Multiple phases will have occurred before a crack becomes visible, and even more before the crack gets to critical lengths. Schijve uses Figure 2.1 to show the different phases and to make distinctions between them [9]. According to Schijve, fatigue cracks nuclei start as invisible microcracks in slipbands. This nucleation of cracks occurs as soon as a cyclic stress above the fatigue limit (limit below which fatigue does not happen) is applied. After nucleation of the microcrack, the growth rate can still be slow, due to grain boundaries and other microstructure effects. Once the crack has grown away from the nucleation site, usually a more regular growth is observed. This will start the process of crack growth. Microcracks become macro cracks and eventually the material will fail due to the cracks becoming too large. Schijve divides the different phases into two periods; the crack initiation period and the crack growth period. As both periods have different variables influencing their behaviour, it is important to differentiate between these two periods. For example surface conditions can have significant effect on the initiation phase, but will not change the growth period significantly. As shown in Figure 2.1 both periods also have different parameters for the prediction of formation and growth. The stress concentration factor K_t is used to predict crack initiation, while the stress intensity factor K is used to predict the growth. The fracture toughness K_{ic} is the maximum value for the stress intensity factor, if that is reached, the crack will grow fast and unstable. The rail will fail. Both the stress concentration and the stress intensity factor will be discussed later in this chapter. The boundary between these two different phases is important to mention. Crack initiation is mainly determined by the material surface phenomenon, where crack propagation depends on the material as a bulk property and is not influenced by the surface phenomenon. One can thus say that if the microcrack growth no longer depends on surface phenomena, then crack initiation becomes propagation [9].
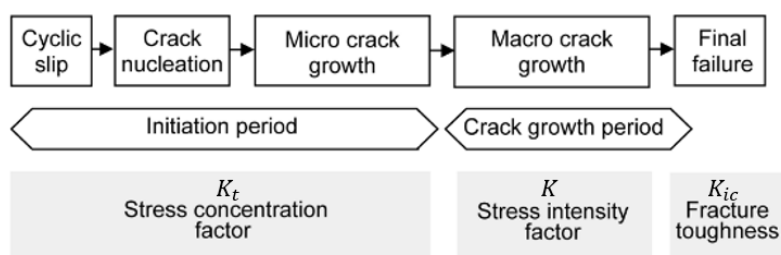
Figure 2.1: *Different phases of fatigue crack formation [9].*

7

For rails, these phenomena mainly come down to very localized stress concentrations due to irregularities in the material. In general, the boundary between crack initiation and crack growth is placed at the point where the crack becomes visible to the naked eye.

2.2   Crack initiation

During the crack initiation phase, the nuclei of the crack is formed. A microcrack slowly finds its way in the material until a sizable crack is developed and steady crack growth is occurring (propagation). Crack initiation starts with cyclic slip, otherwise known as cyclic plastic deformation. As the cyclic stress is generally below the yield stress, this plastic deformation takes place at only a small number of grains in the material. As the grains on the surface of the material are less constrained compared to grains in the material, (less surrounding material) lower stress levels are needed to let slip occur in the grains. If this happens, a slip step will be created (the new fresh surface in Figure 2.2a). Some strain hardening in the slip band will also be developed. Because of this, if the stress during the cycle decreases, a negative shear stress will generate another slip step in adjacent parallel slip planes. This phenomenon is shown schematically in Figure 2.2. When the cyclic stress is applied (a), slip will occur. This will be followed by the stress decreasing with negative shear stress in the material forming another parallel slip band (b). More cycles will repeat this process (c,d,e) with crack initiation as a result [9].
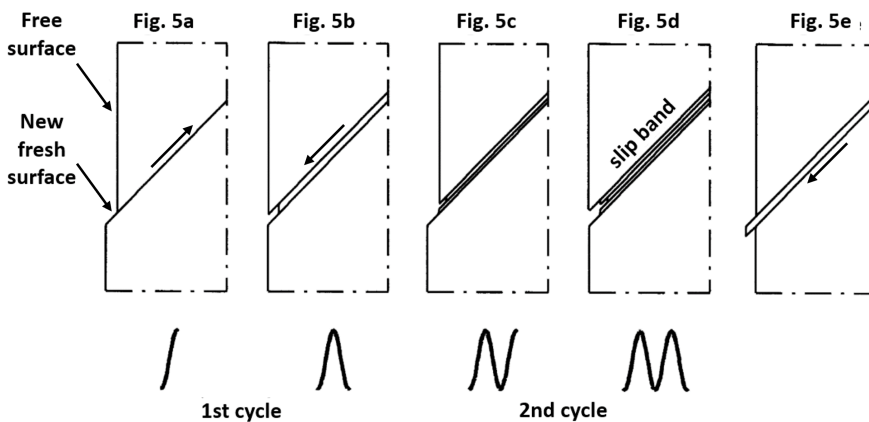
Figure 2.2: *Phases of cyclic slip crack nucleation [9]*

To predict where these cracks will initiate, the stress concentration factor K_t can be an important factor. This dimensionless factor is defined as the ratio between a peak stress due to a discontinuity and the nominal stress [10]. In geometries with holes, flanges, fillets or other features, the stress in the material could be disrupted, creating a high stress concentration around those features and thus a high K_t. For crack initiation, this factor is useful as the location of the stress concentration could predict the location where cracks are formed. As for this research, mainly crack formation on the top of the rail is observed, it can be assumed that geometry does not play an important role in determining the role of the initiation. As high, concentrated loads are placed on the rail when a train axle crosses the rail, it is evident that stress concentrations are highest in the area surrounding the contact area, where thus K_t is high.

Especially when train axles cross the rail at exactly the same points continuously, there is a high chance that micro defects in the material will grow out to become cracks. In Section 2.4 an overview of potential models to predict this crack initiation is given.

2.3   Crack Growth

Once the crack is initiated and has grown to visible lengths, the crack gets into the growth phase. This transition length is assumed to be in the order 1-3 mm. As crack growth prediction is primarily dependent on the sort of fracture mechanics theory used, some more explanation about this will be given.

2.3.1   Fracture Mechanics

In fracture mechanics [11], fracture-dominant failure is the main source of interest [12]. In 1920, Griffith was the first to study the propagation of brittle cracks in glass. He stated the concept that if the energy release rate G of a body per unit new crack area, which would occur for infinitesimal crack extension, is equal to or greater than twice the increase in surface energy γ, a crack will grow [13]. This concept is described as $G \geq 2\gamma \rightarrow$ *crack growth possible*. After this first step in fracture mechanics, Irwin [12] made major advances in this field by introducing a stress intensity approach. He showed that stresses in the vicinity of a crack tip take the form

$$\sigma_{ij} = \frac{K}{\sqrt{2\pi r}} f_{ij}(\theta) + H.O.T., \tag{2.1}$$

where r, θ are cylindrical polar coordinates of a point close to the crack tip (see Figure 2.3). $f_{ij}(\theta)$ is a dimensionless expression dependent on θ only. K gives the magnitude of the elastic stress field. This parameter is called the stress intensity factor. Dimensional analysis suggests that K is linearly related to stress σ and directly to the square root of the crack length a. From this, the general form of the stress intensity factor is given;

$$K = \sigma\sqrt{\pi a} \tag{2.2}$$

Griffiths Energy release theory can be combined with this stress intensity factor and the Youngg's Modulus E given by the relation;
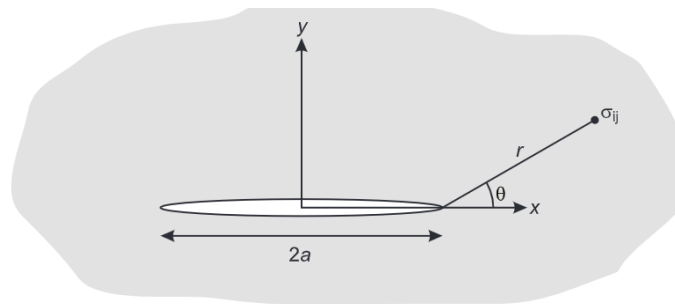
$$G = \frac{K^2}{E} \tag{2.3}$$

Figure 2.3: *Stress at a point near the crack tip [12]*

Using Equation (2.2) and a critical value for the stress intensity K_C, the fracture toughness, it can be said that if $K > K_C$ then crack growth will occur. This statement has become one of the fundamental principles of Fracture mechanics, specifically for Linear Elastic Fracture Mechanics (LEFM), from which Elastic Plastic Fracture Mechanics (EPFM) is a successor. These will be discussed in the next chapter.

2.3.2 Linear Elastic Fracture Mechanics

For LEFM, the use of the stress intensity factor to determine crack growth is the fundamental principle. Equation (2.2) is the base for this approach. For LEFM, the assumption is made that material under load acts primarily in an elastic way. The stresses on the crack are generally divided into three different loading modes with each having an individual stress intensity factor (SIF). In Figure 2.4 an overview of these modes is shown.

(a)   (b)   (c)
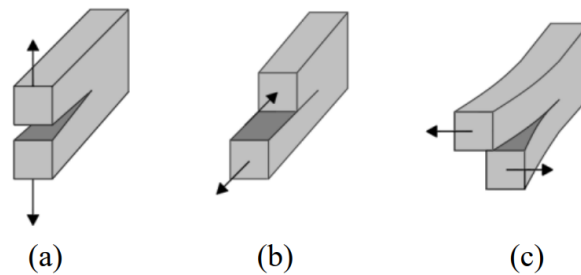
Figure 2.4: *Basic loading modes for cracks (a) opening, (b) in-plane shear, (c) out-of-plane shear [14]*

As for most cases, opening displacement is the most significant loading condition, and this phenomenon is studied the most. In 1968 Paris and Erdogan [15] came up with an expression to express the crack growth rate ($\mathrm{d}a/\mathrm{d}N$) using the stress intensity factor.

$$\frac{\mathrm{d}a}{\mathrm{d}N} = C(\Delta K)^n \tag{2.4}$$

In this equation, C and n are empirical constants. Using this formula and further experiments, they were able to come up with a graph showing the overall development of a crack, see Figure 2.5. In region 1 the crack is formed and initiated. At a certain threshold value for K, the crack starts to grow. This is ΔK_{th}. When moving to region 2, the crack growth starts to increase in a linear matter. The Paris law, Equation (2.4) describes this slope. Eventually the crack growth rate increases faster compared to the derived slope. Once this starts happening, region 3 is reached and only limited number of cycles are needed before the fracture toughness K_C is reached and the crack will fail. Although the Paris Law does not describe the full crack propagation phase, it is used extensively to describe and predict the stable growth (part 2) of the crack formation.

2.3.3 Elastic-Plastic Fracture Mechanics

Because LEFM is only applicable to elastic materials, it is not always possible to describe crack propagation using this method. When relatively large parts of a material are plastically deformed before crack propagation occurs, LEFM is no longer valid. Therefore, Elastic-Plastic Fracture Mechanics (EPFM) approaches have been developed to analyse elastic-plastic materials. To analyse crack growth in these materials, generally two approaches are used; the J integral and the Crack Tip Opening Displacement (CTOD).
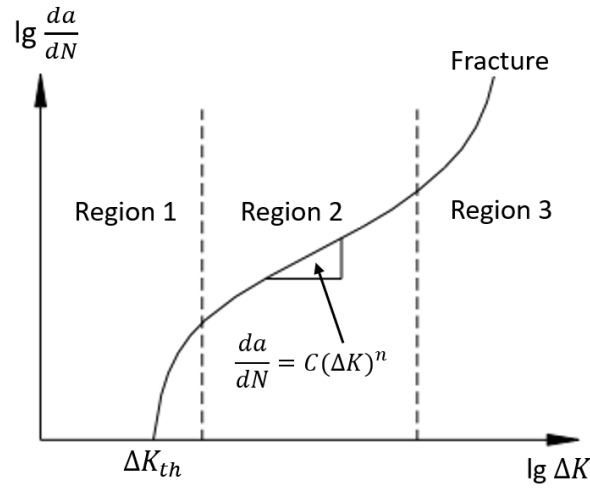
Figure 2.5: *Typical fatigue crack growth curve [16].*

The J integral is defined as the contour line integral which is independent of the integration path. If the critical Value J_{Ic} is reached, cracks start to form. J can be described as follows;

$$J = -\frac{1}{B}\frac{dU}{da} \tag{2.5}$$

where B is the material thickness, U potential energy and a crack length [17].

The resistance of a material to the propagation of a crack is analysed using CTOD. It is calculated by using the geometry of the crack with crack length a, width of the specimen b, dimensionless rotational factor ρ and the crack opening CTOD_m [18].

$$\text{CTOD} = \frac{\rho b}{a + \rho b} \tag{2.6}$$

To accurately describe the ductile behaviour of the railway tracks, a crack growth model based on these kinds of parameters could thus be used. In this report, the primary focus will be on using LEFM approaches, but for some models EPFM factors are used.

2.4 Crack prediction models

In previous sections, an understanding of the crack formation is given and a distinction is made between the crack initiation and crack growth phase. To predict when a crack initiates and grows, models should be used. Although it is possible to get an idea of crack growth by performing experimental results, it is chosen to use numerical models. As numerical models are faster and more easily to implement compared to experimental methods, these are beneficial. Therefore, an overview of possible numerical models regarding initiation and propagation are given in this section.

2.4.1 Crack initiation models

For crack initiation models, it is important to find the location where the crack initiates, as well as the number of cycles until a certain threshold is reached, and thus, the crack is initiated. Where cracks exactly initiate is a factor that is difficult to predict, as it is an inherently stochastic process. From the experiments from Burstow [4],

it is known that cracks predominantly exist at +/- 20 mm from the railhead center laterally, but longitudinally it can not be precisely said where the cracks will grow. From metal microcracks it is known that they generally initiate at peaks of surface roughness or at microstructural inhomogeneities [19]. Because of this pronounced influence of the microstructure, crack initiation can be considered as a stochastic process. An initiation probability could be used to characterize the number of cracks initiated after a given number of load cycles. Multiple researches have tried to come up with a stochastic model describing crack initiation in steel. Such a model could be derived by simple empirical investigations of crack development on a specimen, as Goto [20] did. Ihara and Tanaka [21] did analytical research and came up with a model to calculate the number of cycles up to crack initiation based on the formation of slip bands. This happens if accumulated energy in the material exceeds a specified value. This model takes parameters as dislocation density, grain size and some other microscopic and macroscopic parameters into account. For rails specifically, these models are somewhat more scarce. One of the most promising in this matter is the Brick model, explained in more detail later.

In his thesis, Krishna [22] describes and compares multiple crack initiation models. He divides rolling contact fatigue models into three different kinds of models; Energy dissipation-based, Stress-based and Shear strain-based models. Next to these distinctions, Krishna quantifies the different models utilizing system complexity and damage model complexity (See Figure 2.6). The system complexity relates to how detailed the wheel-rail system is portrayed. If variables like vehicle suspensions, wheel profiles or curve radii are not taken into account, the system complexity becomes far less complex. For rails, it is beneficial to quantify damage by the tonnage passing, that is the amount and weight of trains passing. If the damage complexity is relatively low, the assumption is made that the model is only valid for a limited number of loading cycles or tonnage passing, as the model will not evolve. If the model becomes more complex, effects from material removal are intertwined in the model, making it valid for a larger number of tonnage passing. Finally, if the model is also able to include intermediate maintenance effects, the full operational life can be described, making the model the most complex. The damage model complexity depicts how detailed the physical phenomena behind RCF can be modelled. Relatively simple models see the contact area between the wheel and rail, the contact patch, as a whole. More elaborate models discretize this contact area into more smaller areas to analyse. Finally, the most complex damage models also discretize the material beneath the contact surface, such that sub-surface stresses can be taken into account. Most of the models can be expanded to become complex for either damage or system, however, that would increase calculation lengths and difficulties.

In Figure 2.6 the Whole Life Rail Model has a low damage model complexity but a high possible system complexity [23]. This means that the WLRM is able to describe cases with a broad spectrum of different varying parameters (friction coefficient, wheel profile, axle load, etc.) but only looks at the whole contact patch and is not able to very precisely predict where cracks will initiate. The WLRM is an energy dissipation-based model. The contact energy dissipation is used to determine the damage increment per loading cycle (ΔD_i) for the whole contact patch. As the whole contact patch is seen as one part, it is considered a relatively simple 'global contact' damage model. On the other hand, all kinds of different possible cases can theoretically be studied with this model. An ideal WLRM would be able to include multiple variables and parameters (friction coefficient, rail curvature, etc). Once the WLRM is made, it is straightforward to determine the damage values.
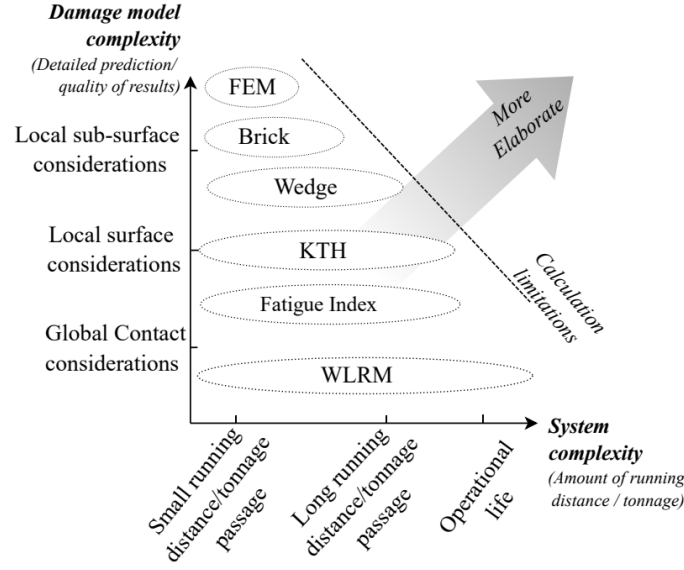
Figure 2.6: *RCF damage model quantification based on model and system complexity[23] .*

Under the stress-based models, methods relating to the shakedown theory are considered. The Surface Fatigue Index model (FI_{surf}) from Ekberg et al. [24] is one of these methods. A working point WP is identified for a given contact load on a shakedown diagram in this model, see Figure 2.7. The Fatigue Index FI_{surf} is described as the shortest distance between working point WP and the boundary curve BC. If this distance is greater than 0, fatigue is expected. FI_{surf} is expressed as

$$FI_{surf} = \mu - \frac{1}{\lambda} \Rightarrow \frac{\sqrt{F_x^2 + F_y^2}}{F_z} - \frac{2\pi abk}{3F_z} \tag{2.7}$$

It is important to mention that the fatigue life is not calculated with this method. In order to get an indication of the fatigue life, a power law could be adopted to describe Damage D, where δD_i is the damage increment per loading cycle. By curve fitting of test results from three bench tests the following estimation was found [24];

$$\delta D_i = \frac{1}{10} FI_{surf}^4 \quad \forall \quad FI_{surf} > 0 \tag{2.8}$$

Instead of a Fatigue Index, one could also consider using the Stress Index SI as a possible approach [25]. This stress index is denoted as:

$$SI(x,y) = \sqrt{\tau_{zx}(x,y)^2 + \tau_{zy}(x,y)^2} - k \tag{2.9}$$

The advantage of using the Stress Index is that stress is calculated for each element instead of considering the contact patch as a whole. Similar to the Fatigue Index, for the Stress Index, a power law relationship is assumed to estimate the damage per loading cycle:

$$\Delta D_i = \alpha'(SI_{\max})^{\beta'} \tag{2.10}$$

where α', β' are material parameters.
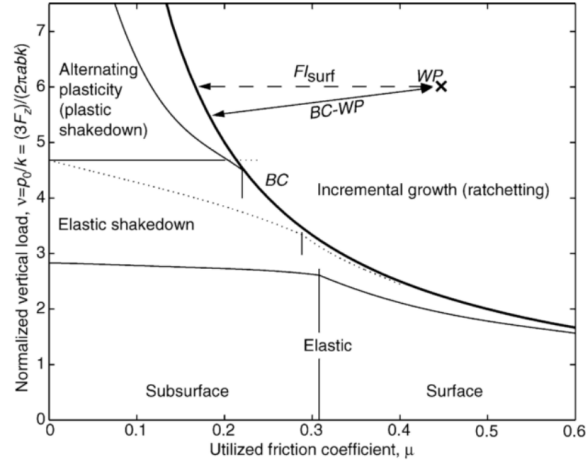
Figure 2.7: *Shakedown diagram used for surface fatigue index model [23].*

For the last type of models, shear strain-based models, critical strain is calculated, such that sub-surface damage can be taken into account. One of these models is the brick model, developed by Franklin et al. [26]. For this model, the cross-section of a rail is modelled as a mesh of elements or bricks. For each individual brick the shear stress fields can be calculated for each loading cycle. In this way the incremental strain can be calculated for each cycle, such that it can be determined when the shear strain of a brick reaches a certain critical threshold and fails. Based on surrounding bricks, the failed brick is either removed as wear or stays and cracks are formed.

Finally, the wedge model, which uses the 'effective stress' σ_A as a damage indicator [27], can be used. This stress is determined with a similarity parameter f_a, traction parameter f_T and maximum principal stress σ';

$$\sigma_A = \max(\sigma')f_a f_T \tag{2.11}$$

Again, a power law is used to estimate damage increment;

$$\delta D_i = \left(\frac{\sigma_A}{\sigma_f}\right)^{\frac{1}{b}} \tag{2.12}$$

where σ_f and b are material dependent constants.

2.4.2 Crack propagation models

To predict the crack growth and the number of cycles until critical crack lengths are reached, crack growth models should be used. Most of these models are based on the Paris law (Equation (2.4)). This equation shows that if the stress intensity factor of a crack can be found, then the crack growth rate can be determined. Once the growth rate is known, the fatigue life can be calculated, assuming the critical crack length is known. Important to mention here is that the crack growth rate changes during crack growth, as shown in Figure 2.5. The Paris law only takes region 2 of this graph into account. It only looks at the linear growth of the crack. To take into account also (part of) the other regions, it could be considered to use modified crack growth laws such as for example the Nasgro equation [28]. These equations will also include (part of) Region 1 and/or 3 of the growth rate, and will thus give a more detailed prediction.

Another point of consideration is that in the Paris law only the stress intensity factor for crack opening displacement is taken into account. The other two modes, in plane shear and out of plane shear, could also be of importance and thus have to be included somehow.

By integrating the Paris Law (Equation (2.4)) the number of load cycles until failure can be estimated. By using an analytical solution, an estimation of the propagation life can be made. The problem however is that the stress intensity factor K depends on the crack length and geometry of the structure. For more complicated geometries, such as rail profiles, analytical integration is not viable. Therefore, crack propagation problems are often solved using computational methods [16]. Methods such as the boundary element method (BEM), the finite element method (FEM), the extended finite element method (XFEM), the element-free Galerkin method (EFGM) and combinations of these have been developed to model and simulate fatigue crack growth [29]. Using these methods, the crack propagation is solved step-wise. For each step, the crack is advanced in a small length, whereafter the number of cycles for the next increment is estimated using a crack propagation law (Paris law). This process is repeated until a critical crack length or a critical stress intensity factor is reached.

The use of FEM for fracture mechanics and the analysis of stress fields for crack growth is well known. For crack growth in rail profiles, Bogdanski et al. [30] developed a 2D FEM model to obtain stress intensity factors and investigate the influence of different friction coefficients, traction loads and residual stresses. They found the traction to be of little influence while the growth rate would decrease for larger friction. Nejad et al. [31, 32] used FEM to analyze wheel-rail interaction and the stress distribution in the rail. They obtained the stress intensity factor K and used a modified Paris law to obtain the crack growth rate. To use FEM for crack growth modelling, 2D or 3D models of the rail are developed and discretized by meshing the model. Pre-defined material properties, forces and constraints on the rail are given as input for the model. Next to that, to allow crack growth, an initial crack location and length are given. Typically for FEM crack modelling, a rosette pattern mesh (see Figure 2.8) is modelled around the crack tip. Around the crack tip, wedge elements (singular elements) are used to model the crack tip singularity and improve the accuracy of the FE results [33]. These results can be used to obtain the stress intensity factors. Generally, two numerical methods are used to extract these, known as displacement matching methods and energy-based methods. Alshoabi and Fageehi [34, 35] made use of a displacement model for describing crack growth in a 2D compact tension specimen (no rail steel). The stress intensity factors could be described as:

$$K_I = \frac{E}{3(1+\nu)(1+\kappa)}\sqrt{\frac{2\pi}{L}}\left(4(v_b' - v_d') - \frac{(v_c' - v_e')}{2}\right) \tag{2.13a}$$

$$K_{II} = \frac{E}{3(1+\nu)(1+\kappa)}\sqrt{\frac{2\pi}{L}}\left(4(u_b' - u_d') - \frac{(u_c' - u_e')}{2}\right) \tag{2.13b}$$

where E is the modus of Elasticity, ν the Poisson's ratio, L the quarter-point element length and κ the elastic parameter defined by

$$\kappa = \begin{cases} 3 - 4\nu & \text{for plane strain} \\ \frac{(3-\nu)}{(1+\nu)} & \text{for plane stress} \end{cases} \tag{2.14}$$

The u' and v' are displacement components in the x' and y' direction respectively. The subscriptions represent their position, as shown in Figure 2.8.
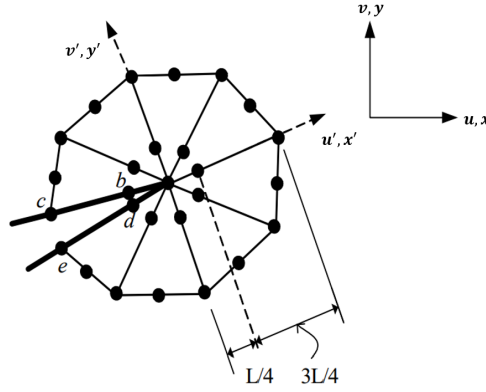
Figure 2.8: *Quarter-point singular elements around crack tip [35].*

When using an energy method, it is common to identify the energy release rate, G, or a similar output. The energy release rate is defined as the potential energy decrease per unit crack advance.

Although FEM is a popular method to analyse these kinds of structural problems, it is a challenging process to perform for crack propagation. This challenge lies in the fact that for each step when the crack is advanced, the finite element mesh has to be updated. To overcome this issue, other methods, such as BEM, EFGM and XFEM were developed [16]. In general, for these methods, a basis lies in finding the energy release rate. For 2D problems, Rice [36] showed that the energy release rate can be computed by a path-independent line integral given by:

$$J = \int_\Gamma W(x,y)dy - \int_\Gamma T \cdot \frac{\partial u}{\partial x}ds \tag{2.15}$$

where Γ is the curve surrounding the crack tip, $W(x,y)$ is the strain energy density field and x,y are the cartesian coordinates being parallel and normal to the crack tip, respectively. T is the traction vector outward, normal to Γ, u is the displacement vector and ds is the incremental arc length along Γ. To compute the stress intensity factors, this equation can be evaluated numerically for the FEM solution over an arbitrary path around the crack tip. For LEFM problems, it can be said that $J = G$. The stress intensity factors can thus be related to the energy release rate by:

$$K_I = \sqrt{GE} = \sqrt{JE} \tag{2.16}$$

Because this method is based on a path around the crack tip, in 3D it is difficult to perform the same routine as the integral then becomes a surface integral. Because of this, a domain integral method was developed by Shih et al. [37]. They used a divergence theorem to compute the J integral. In this, the three-dimensional surface integral is transformed into a volume domain integral, which is evaluated by Gaussian quadrature. To be able to extract the stress intensity factors for all three crack modes, Equation (2.16) does not suffice. When all three SIFS are taken into account, an equation with three unknowns would arise, which is not solvable. A technique involving an interaction integral was developed by Yau et al. [38], which avoids this problem. In words, this technique comes down extending Equation (2.16) such that all Stress intensity factors are involved. The J integral is calculated for multiple auxiliary stress fields, such that a system of multiple equations arises that is able to solve for the stress intensity factors.

Once the stress intensity factors have been found, the Paris law can be used to obtain the crack growth rate. As explained before, the crack propagation is solved step-wise with small crack size increases. The difficulty with using FEM for crack growth lies in this step, as for each increment, the mesh around the crack has to be removed and replaced such that the rosette pattern mesh is once again around the tip. This is a time-consuming job and therefore XFEM has been used in certain instances to predict crack growth. XFEM can predict crack growth independent of the mesh and re-meshing is not necessary. While XFEM still computes the displacement and stress fields of the given model, it can include crack growth in this calculation. By enriching the finite elements that are cut by the crack, the discontinuity of and singularity around the crack is taken into account. In the displacement field calculation for XFEM, one can therefore see an extra term added to the equation, which takes into consideration these enriched nodes.[39]

After the XFEM solution is found, the stress intensity factors are found in a similar way to the FEM model, by employing the domain form of the interaction integral. For crack propagation in railway tracks, Rodriguez-Arana et al. [40] have used XFEM to obtain shear stresses and stress intensity factors of tracks with semi-elliptical pre-cracks. Bobis et al. [41, 42] have done similar research with 2D and later 3D models to estimate lifetime based on the Paris' law. Because of the added advancements of XFEM compared to FEM, it is proposed to model the crack growth in this paper using XFEM.

In this chapter, the crack formation was divided into initiation and propagation. For both, the theory behind their occurrence was explained. Eventually, multiple initiation and propagation models were discussed. For the initiation, models such as the Fatigue Index and the Stress Index were discussed. Both are relatively easily calculated if forces or stresses are known. The disadvantage of these models is their relative simplicity. an exact crack location is not found and coupling these models to location-specific parameters such as the cof or the train speed is difficult. The brick model is seen as a more promising model, as the exact location of the crack in the rail is analysed. Even though this model takes more time to calculate the crack initiation, more precise results can be obtained. The number of cycles before a certain bricks fails could then be used as N_{in}. To analyse the propagation of cracks, FEM models are shown to be valuable. Especially XFEM models are promising due to their advantage of modelling a propagating crack without having to remesh. For these models, the number of cycles until a certain critical crack length can be used to determine N_{prop}.

After discussing initiation, propagation and their possible prediction models, it was decided to focus on propagation first. Because it is expected that propagation has the highest influence on the RCF curve of the WLRM, this phase of the crack growth is seen as the most important. From the Initiation phase, it is expected that this will mainly influence the threshold value of the RCF curve, where the propagation phase will also influence the slope. In the next chapter, the propagation modelling using XFEM will be discussed.

3 | Methodology

In the methodology, the steps taken to reach the research objectives are explained. In Chapter 2, crack formation is described and a distinction has been made between crack initiation and crack propagation. In the last chapter, the choice is made to focus on crack propagation first. Therefore, the model describing this propagation will be discussed in this chapter.

3.1 Crack propagation model

In the literature review, a few propagation models have been discussed. As explained, XFEM is commonly used and a proper method to asses crack propagation in steel. Even though only limited studies are performed using XFEM for rail cracks, the ability of fast crack propagation analysis was the reason why it was chosen to continue using XFEM. As rails are made of steel, it is presumed that the XFEM method will be applicable to rail cracks. The XFEM capabilities of Abaqus are used to perform this research. Abaqus describes XFEM as an analysis which makes it possible to study crack growth along an arbitrary, solution-dependent path without needing to remesh the model. In this Abaqus XFEM implementation model, it is possible to either specify the crack location yourself or let Abaqus determine the crack location based on maximum principle stress or strain [39]. To perform this analysis, the user has to define the crack domain. For a three-dimensional part, this domain is defined as the cells in which the crack could propagate. The user also defines if the crack can propagate or if it stays stationary. Finally, if the user chooses to define an initial crack location, a face has to be selected. This can be a face of the solid model, a face created by partition or a face from another planar part instance [39].
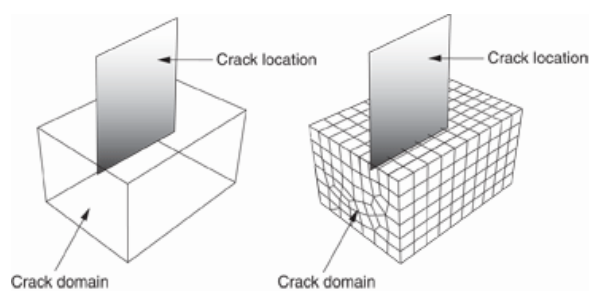
Figure 3.1: *Crack domain and location for Abaqus XFEM [39].*

Once the part model and the crack have been defined, the fracture mechanics theory is used to evaluate stress and strain fields ahead of the crack tip. By default, the stress/strain at the element centroid ahead of the crack tip is computed. If a pre-defined maximum stress or strain is exceeded, the crack grows and its direction is determined. For this method, a sufficiently refined mesh around the crack tip is necessary, as otherwise the approximation of the stress and strain field at the element centroid compared to the crack tip may not be sufficient [43]. Using these stress/strain components, crack growth and propagation can be determined.

3.2   Model Development

An Abaqus XFEM model was build which is used to validate the model and show the possibilities of this model. A piece of rail was modelled in Abaqus based on the work of Rodriquez et al. [40]. Rodriquez showed that, for a vertical load of 100 kN, the piece of rail in the model needed to be at least 6000 mm. With shorter lengths, the numerical results would be influenced by the length of the rail. Because of this, a rail of the same length was taken as input for this model. At the underside, the rail was constrained by elastic foundations with a stiffness of 75 kN/mm, which is similar to the stiffness used by Rodriquez and the average stiffness of a sleeper taking into consideration concrete and composite sleepers [44] (wooden sleepers generally have stiffnesses similar to composite sleepers). These foundations were placed with 600 mm distance between each other to model the sleepers. apart from the vertical direction, the rail was constrained in all other directions. At the top of the rail, laterally in the middle, a semi-elliptical crack was placed, as this is a commonly used crack shape in XFEM modelling. According to Mai et al. [45], it has no significant influence on the second Stress Intensity Factor (in-plane-shear) if the crack is placed between sleepers or on top of sleepers. Because of this, the crack could be placed anywhere. In the developed model no significant difference was found either. For convenience, the crack was placed in the middle of the model, between two sleepers. A simplified drawing of the model with its sleepers and the predefined crack is shown in Figure 3.2. In this Figure, the orange half-circle is modelling the train wheel running over the rail. In the Abaqus model, this is a combination of a normal pressure and a shear stress moving over the rail. Figure 3.3 shows the middle part of the track with the circular crack in red.
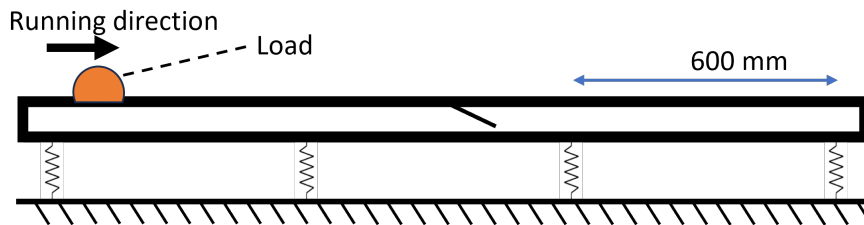
Figure 3.2: *simplified model.*

In order to validate the model and check if similar results are found, the model was compared against the work of Mai et al. [45] and the work of Rodriquez et al. [40]. The load, contact patch and crack are described in Table 3.1. The normal load is described as a semi-ellipsoid with maximum pressure P_o in the middle. The traction load is given by $T = P_o \mu$. A visualisation of both loads is given in Figure 3.4.

Table 3.1: *Load and crack parameters.*

Normal Load P_o (MPa)	Friction Coefficient μ	Semi-axis Long. a (mm)	Lat. b (mm)	Crack Length A (mm)	Width B (mm)	Angle θ (deg)
1570	0.1	7	4	6	6.6	75
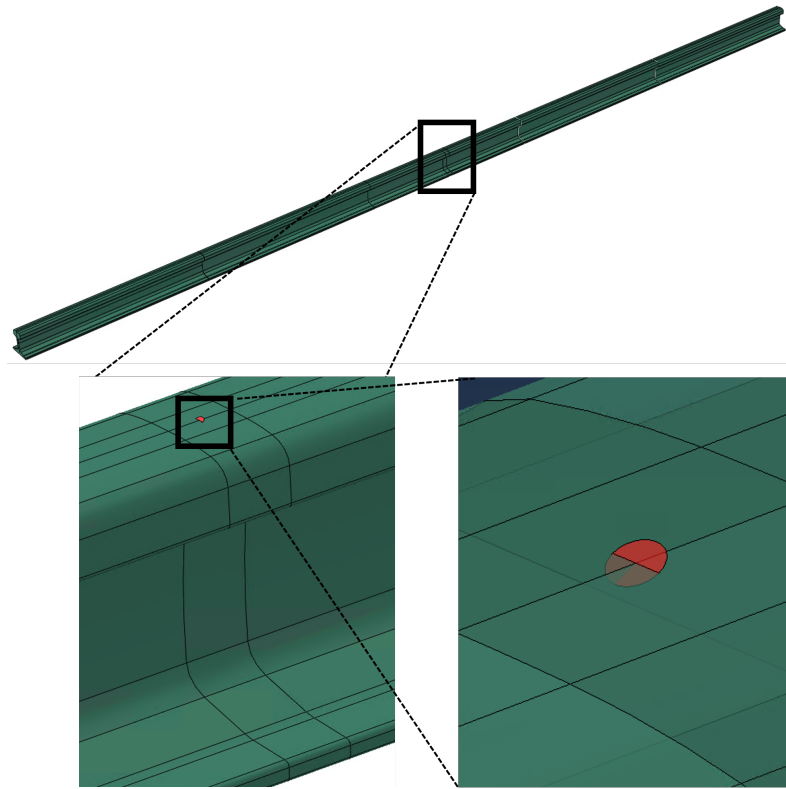
Figure 3.3: *Abaqus FEM model with crack situated at the center.*
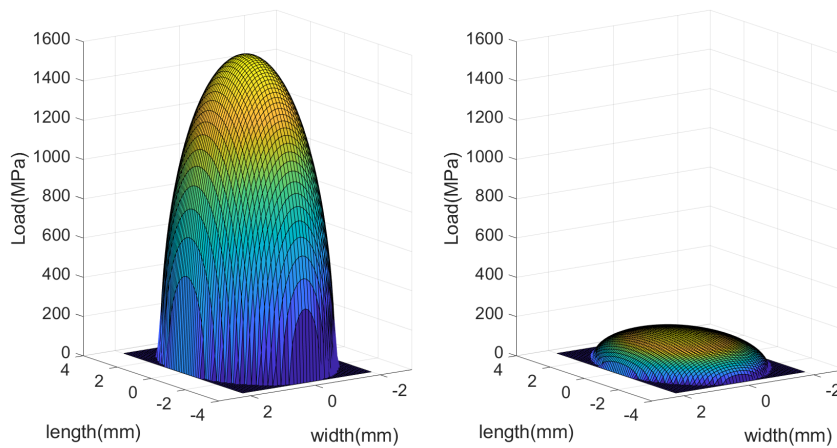
Figure 3.4: *visualised normal (L) and traction load (R).*

To compare this model with previous work from Rodiquez and Mai [40, 45], the stress intensity factor at the crack tip has to be found. These are calculated by Abaqus and used as the output of the model. To be able to get these results, the crack has to be kept stationary. This means that, during the load cycle, the stresses at the crack are computed but no growth is occurring. An interaction integral approach is used to find the J integral in Abaqus. This integral is then used to obtain the SIFs for mixed-mode loading. This approach is explained in more detail in the next section.
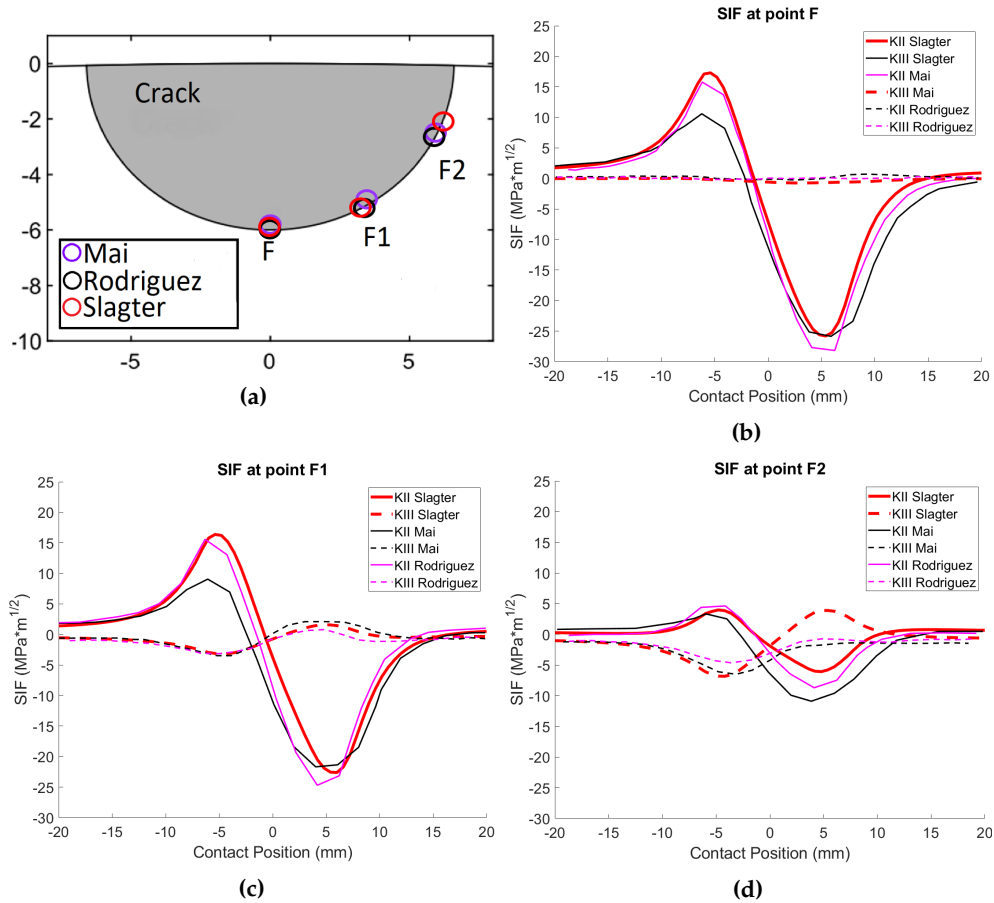
Figure 3.5: *Comparison of SIF at point F (a), at point F1 (b) and point F2 (c) around the crack tip (d).*

Using this model, the Stress Intensity Factors at the crack tip were calculated and compared with the other works. Three points in the semi-elliptical crack were used to compare SIFs of this research model with the model from Rodriquez and the model from Mai. The three measurement points are shown in Figure 3.5a. As the locations where the SIFs can be measured are dependent on the used mesh, it was not possible to coincide exactly with the locations from Rodriquez and Mai. Especially for point F2 there is a small offset. In Figures 3.5b to 3.5d, SIFs K2 and K3 for the three models are compared to each other. At contact position 0 mm, the load is exactly on top of the crack. For point F and F1, the similarities between the three different models are considered small enough to be viable. For point F2 the value of K3 is higher after crossing the crack. This small deviation is expected to be the case because of the offset from the measuring points.

3.3   Model setup

Once the Abaqus model has proven to show similar results compared to previous research, the theory can be used to set up the system to be able to calculate the Damage index for the WLRM by using VI-Rail simulation results as input. Multiple steps have to be taken to transform VI-Rail data to usable results for the RCF function. In Figure 3.6 an overview of these steps is given. The data from the VI-Rail simulations is used in Matlab to determine pressure and traction fields. Using Fortran,

these loads are placed in the Abaqus model. This Abaqus model will simulate a cycle and determine stresses and corresponding SIFs in the crack tip. These SIFs are used to determine crack growth rate, and eventually, a damage index based on a critical crack length. On the other side, a wear number has to be obtained, which can be calculated using VI-Rail data. By following all steps, it should be possible to find points in the WLRM for RCF damage. All steps will be discussed in the following sections.
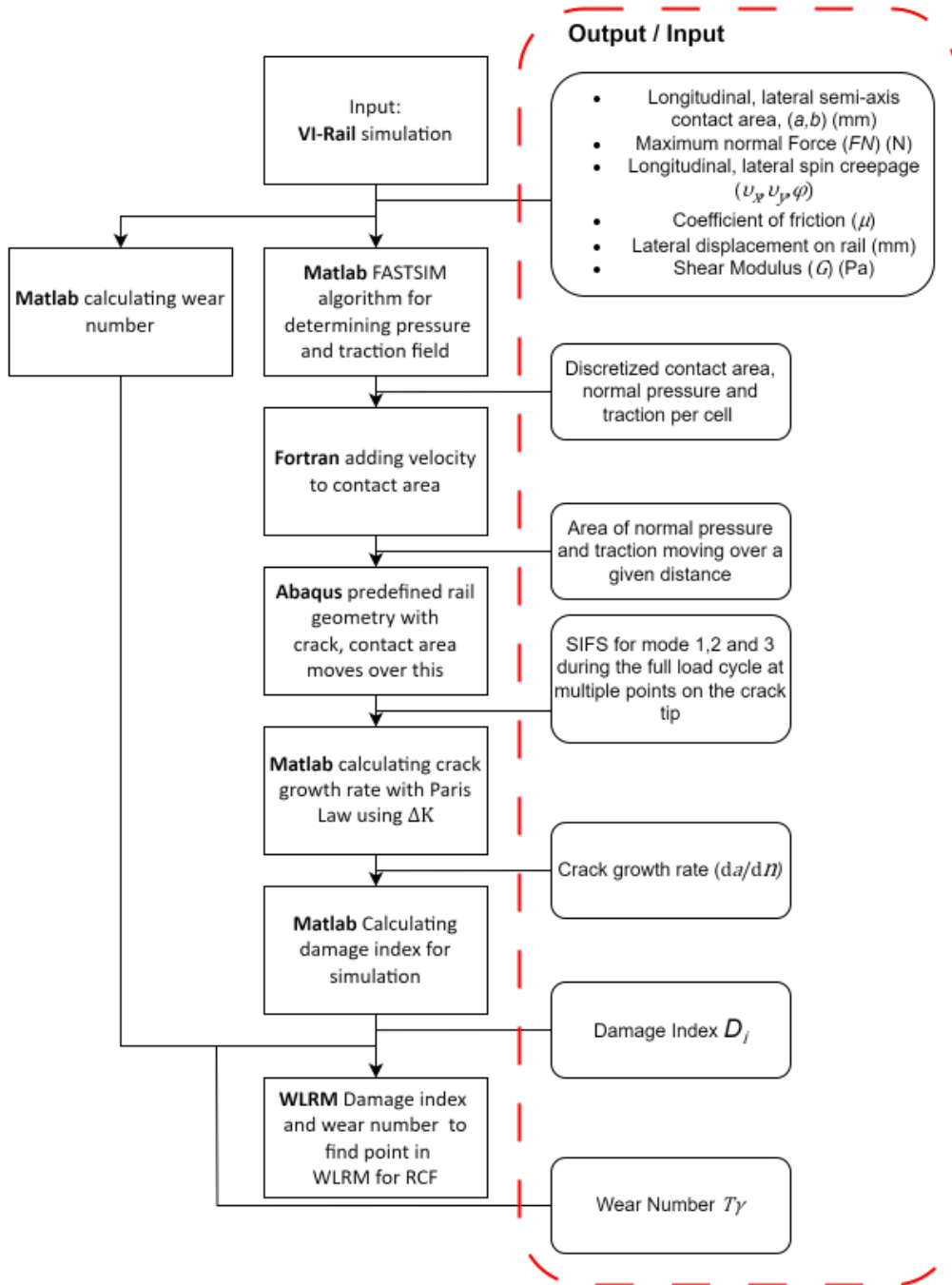

Figure 3.6: *Overview of the steps in the model.*

3.3.1 VI-Rail input

The first step in the model is the input of the VI-Rail data into the model. To be able to calculate the load and traction in the next step, the contact area, normal force, longitudinal creepage, lateral creepage, spin creepage and friction coefficient have to be obtained. In the model, the assumption is made that the crack will form precisely below the contact patch. The lateral position of the contact patch relative to the rail can differ. As the train is pushed to the outside with a certain centrifugal force, the lateral displacement of the wheels relative to the rail can be different for different simulations. Because of this, this displacement is also taken as input for the model. The initial crack will be placed at the lateral position where the wheel passes the rail. Figure 3.7a schematically shows the rail with a red arrow pointing to the contact patch and a green arrow showing the possible movement of this contact patch. The VI-Rail simulation data generally exists out of 10 to 30 seconds of simulation data with time increments of 0.01 seconds. In the simulations used for this research, the simulation generally exists out of a train running over a straight piece of track which changes gradually to an arch with a certain radius. Because crack formation commonly takes place in arches, it is chosen to take data from one of the last data points of the simulation data. Here, the train is still in the arch but has settled to relatively stable contact properties. In Figure 3.7b a schematic overview of the track geometry is shown
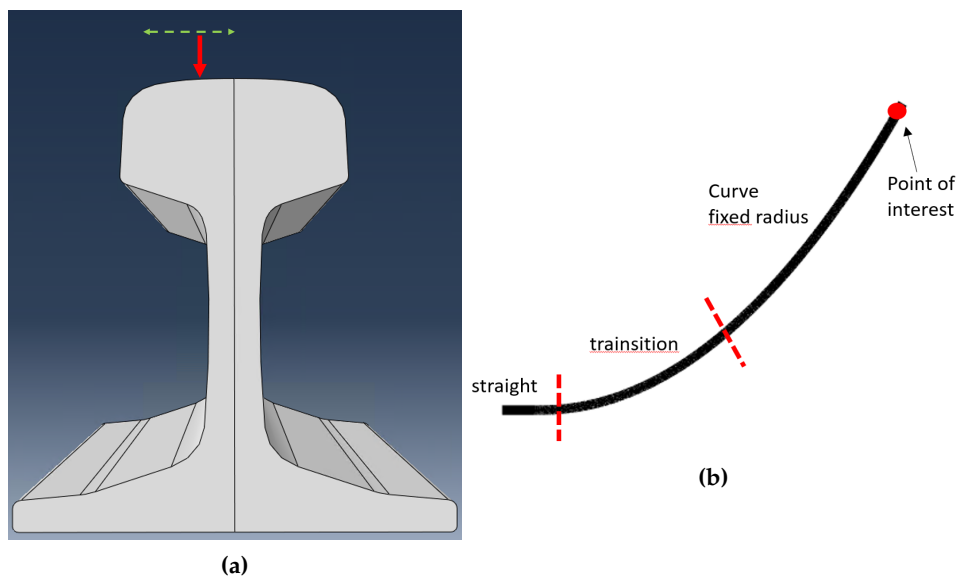
Figure 3.7: *Lateral and longitudinal placement of location of interest.*

3.3.2 Matlab FASTSIM

Once the input values are clear, these have to be translated to contact parameters that can be used in the Abaqus model. To find the pressure and traction field, the FAST-SIM algorithm is used [46]. The theory behind this algorithm is based on Kalker's simplified theory, who used the strip theory to come to his conclusions. This strip theory assumes an elliptical contact patch with half-axes a and b. In this theory, there is a slip and a stick zone, and in the stick zone the tangential stress distribution is changed compared to simple parabolic behaviour.

For 3D cases, the contact patch is divided into strips parallel to the rolling direction and treated individually. Figure 3.8 shows an overview of the strip theory. The yellow strip is one strip with half length of the contact patch $a(y)$ and half length of the slip zone $d(y)$.
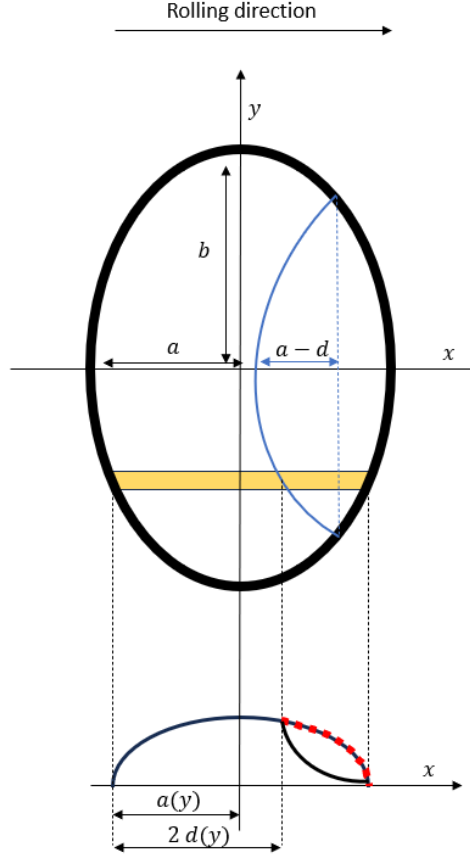
Figure 3.8: *Overview of the strip theory.*

Based on the strip theory, Kalker made up his complete theory of rolling contact, which eventually led to the simplified theory (due to the high computational efforts of the complete theory). In the simplified theory, a linear relationship between surface deformation and traction is assumed:

$$\boldsymbol{u} = L\boldsymbol{\tau} \qquad (3.1)$$

with $\boldsymbol{u} = (u_x, u_y, u_z)$ being the deformation vector $\boldsymbol{\tau} = (q_x, q_y, p)$ is the traction vector described by the longitudinal and lateral stress and the normal pressure respectively. Finally, L is a flexibility parameter. Because deformation in the normal direction can be found more accurately by the Hertzian contact stress, the part $u_z = Lp$ is omitted. Surface deformations u_x, u_y are found using the spin and creepage $\varphi, \upsilon_x, \upsilon_y$. By adding arbitrary functions f and g as integration constants, u_x and u_y are calculated as:

$$u_x = \upsilon_x x - \varphi xy + f(y) \qquad (3.2a)$$

$$u_y = \upsilon_y x - \varphi \frac{x^2}{2} + g(y) \qquad (3.2b)$$

for full adhesion in steady state rolling. By using $u_x = Lq_x$ and $u_y, = Lq_y$ and assuming the boundary conditions to be $q_x(a(y), y) = 0$ and $q_y(a(y), y) = 0$ at the leading contact edges, the traction distribution can be written as:

$$q_x = [v_x(x - a(y)) - \varphi(x - a(y))y]/L \tag{3.3a}$$

$$q_y = [v_y(x - a(y)) - \varphi(x^2 - a^2(y))/2]/L \tag{3.3b}$$

with $a(y)$ being the half length of the contact patch at y. By integrating these expressions over the contact patch, the total force for both can be described as:

$$F_x = \frac{-8a^2 b v_x}{3L} \tag{3.4a}$$

$$F_y = \frac{-8a^2 b v_y}{3L} - \frac{\pi a^3 b \varphi}{4L} \tag{3.4b}$$

To find an expression for the flexibility parameter L, the linear theory of Kalker [47] could be used. In this, he assumed that no slip is happening. In that case, the creep forces and spin moment can be described as:

$$F_x = -C_{11} G c^2 v_x \tag{3.5a}$$

$$F_y = -C_{22} G c^2 v_y - C_{23} G c^3 \varphi \tag{3.5b}$$

$$M_z = -C_{23} G c^3 v_y - C_{33} G c^4 \varphi \tag{3.5c}$$

with $c = \sqrt{ab}$ and C_{ij} being Kalker coefficients. These coefficients depend on the Poisson's ratio and the ratio between the contact ellipse axes a/b. A table with these coefficients can be found in the work of Kalker [48]. As it is impossible to find a single flexibility parameter for all three equations, three different parameters are set up to apply to each corresponding equation,

$$L_x = \frac{8a}{3GC_{11}} \quad L_y = \frac{8a}{3GC_{22}} \quad L_\varphi = \frac{\pi a^2}{4GcC_{23}} \tag{3.6}$$

Instead of using these three different parameters, one could also consider to use a single weighted parameter:

$$L = \frac{L_x |v_x| + L_y |v_y| + L_\varphi |\varphi| c}{\sqrt{v_x^2 + v_y^2 + (\varphi c)^2}} \tag{3.7}$$

Knowing how the traction distribution is calculated, only the traction bound is still important. This can be found either by using the Hertzian contact pressure distribution times the friction coefficient:

$$\mu p(x, y) = \mu p_0 \sqrt{1 - \left(\frac{x}{a}\right)^2 - \left(\frac{y}{b}\right)^2} \tag{3.8}$$

with p_0 being the maximum pressure at the contact patch described by the contact force N and contact axes (a, b) as:

$$p_0 = \frac{3N}{2\pi ab} \tag{3.9}$$

Instead of using the Hertzian contact pressure, this could also be replaced by a distribution based on the simplified theory in normal direction:

$$\mu p'(x, y) = \mu p_0' \left(1 - \left(\frac{x}{a}\right)^2 - \left(\frac{y}{b}\right)^2\right) \tag{3.10}$$

with

$$p'_0 = \frac{2N}{\pi ab} \tag{3.11}$$

Where the Hertzian distribution is elliptic, the simplified distribution is parabolic, which proved to result in more accurate stick-slip boundaries [46]. However, an algorithm is needed when spin is present to use this simplified theory. One algorithm that can handle this is known as FASTSIM [48]. In this algorithm, the contact patch is discretized into strips parallel to the running direction. Each strip is discretized further into rectangular elements. Figure 3.9 shows such a discretized strip in the contact patch. Shear stress along a strip is calculated as

$$\overline{q}_x^{n+1} = q_x^n - \left(\frac{v_x}{L_x} - \frac{\varphi y}{L_\varphi}\right) dx \tag{3.12}$$

$$\overline{q}_y^{n+1} = q_y^n - \left(\frac{v_y}{L_y} + \frac{\varphi x}{L_\varphi}\right) dx \tag{3.13}$$

with n indicating the sequence of elements in the strip. The total shear stress can be described as

$$\overline{q}_t = \sqrt{\overline{q}_x^2 + \overline{q}_y^2} \tag{3.14}$$

for each element. If this is found to be greater than the parabolic traction bound $\mu p'(x,y)$ the shear stresses have to be recalculated by scaling them to the normal pressure as:

$$q_x^{n+1} = \overline{q}_x^{n+1} \frac{\mu p'(x,y)}{\overline{q}_t} \tag{3.15}$$

$$q_y^{n+1} = \overline{q}_y^{n+1} \frac{\mu p'(x,y)}{\overline{q}_t} \tag{3.16}$$
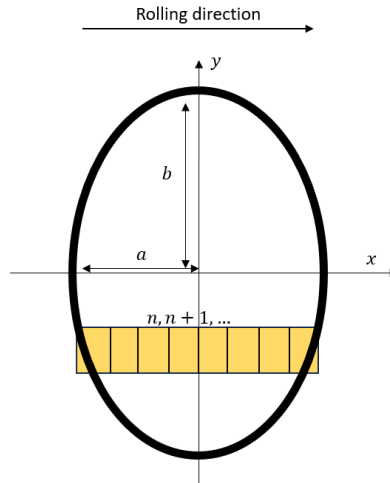
Figure 3.9: *discretized strip for FASTSIM.*

This theory has been implemented in Matlab to calculate the shear stresses at the contact patch. The normal pressure finally is calculated for each element assuming that maximum contact pressure is placed at the centre of the contact area. Pressure at the middle of each element is then calculated as

$$p_{ij} = p_0 \sqrt{1 - \left(\frac{x_{ij}}{a}\right)^2 - \left(\frac{y_{ij}}{b}\right)^2} \tag{3.17}$$

with (x_{ij}, y_{ij}) being the coordinates of the midpoint of the element.
To summarize this step, the contact patch axes (a, b), the normal force N, creepages

and spin (v_x, v_y, φ) are taken from the VI-Rail simulations. Using Equation (3.17) the pressure distribution is calculated. The FASTSIM algorithm is used to calculate the traction distribution. These two distributions will be used in the next steps.

3.3.3 Fortran

Once the pressure distributions are known, a static simulation in Abaqus could be done in which the distribution stays stationary. As the idea of the simulation is to simulate a wheel running over the rail and obtaining the stress variations due to this movement, it would be favourable to perform an Abaqus simulation in which the pressures are moving over the rail. To do this, subroutines have to be used, which have to be written separately from the Abaqus environment and using Fortran language. In reality, this comes down to a separate file which receives the pressure and traction distribution. The centre of the contact patch is taken and a velocity is given to this point. The Fortran code then makes sure that after each time step, the centre point of the contact patch is moved according to the velocity. The contact patch around this node is kept stationary relative to the centre node, such that the contact patch moves in the same manner as the middle node. In Figure 3.10, a visual overview of the Fortran routine is given. The input into Fortran is coordinates for each cell, as well as pressure and traction for each cell. For the center, the coordinate is also given and cell coordinates are related to that such that they stay at the same distance. For each timestep, the x coordinate of the center is calculated by adding the old coordinate to the travelled distance (velocity multiplied by time). The cell coordinates are then updated accordingly. For this research, the velocity is always kept as 0.06 m/s, and one simulation is taken over one second, so 0.06 m is travelled. As the only interest for the simulation is the maximum Stress Intensity Factors, which are occurring when the contact patch is right above the crack, having a longer travel distance is not necessary. The velocity is chosen to be low as this increases the accuracy of the SIF extraction. If higher speeds would be used, smaller time increments and thus more calculation steps would be needed to find similar results. Finally, The crack is always placed in the middle of this travel distance, such that the SIFS during entering, crossing and leaving the crack can be obtained.
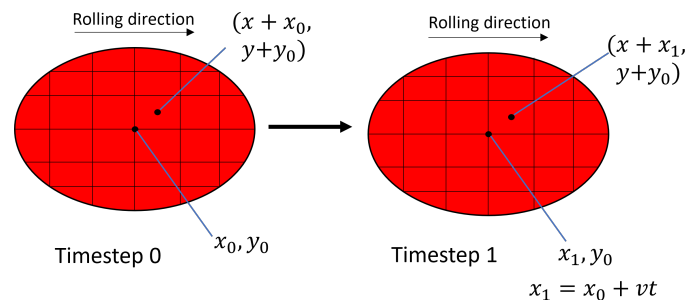
Figure 3.10: *Visual overview of the Fortran routine.*

3.3.4 Abaqus

Once all forces and contacts are defined, these are loaded into the Abaqus model and a static, general step of one second with fixed increments of 0.01s is performed. Smaller timesteps would increase the calculation time significantly while the results would be similar. During this timestep, the loads move over the rail and the stresses at the crack tip are monitored. In order to retrieve the stress intensity factors, Abaqus makes use of an interaction integral method. According to the Abaqus documentation [49], Abaqus first calculates the J-integral such that the energy release rate can

be found and associated to the crack advance. For a two-dimensional case, the J integral can be defined as

$$J = \lim_{\Gamma \to 0} \int_{\Gamma} n \cdot H \cdot q d\Gamma \tag{3.18}$$

with Γ being a contour beginning at the one side of the crack surfaces and ending at the other. With the limit $\Gamma \to 0$ it is indicated that Γ shrinks into the crack tip. q is a unit vector in the virtual crack extension direction, n the outward normal vector to Γ and H is given as:

$$H = (WI - \sigma \cdot \frac{\partial u}{\partial x}) \tag{3.19}$$

For elastic materials W is the elastic strain energy. Otherwise W represents the elastic strain energy density plus the plastic dissipation. In Figure 3.11, a crack with contour is shown. Abaqus defines multiple contours by making contours of elements farther from the crack tip with each additional contour. The length of the contour Γ is thus changed for each contour.
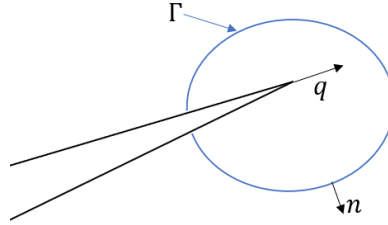

Figure 3.11: *crack with contour Γ.*

For three-dimensional cases, the J integral is more difficult to calculate as the 2D contour becomes a 3D cylinder around the crack. Abaqus nevertheless is able to calculate the J integral for these situations. In this research however, that step is seen as a black box. The next step, the conversion from J-integral to Stress Intensity Factors, is assumed to be in the same black box. In case of plane strain with only Mode 1 loading (crack opening), there is a simple relation between the J-integral and K1 [16] being;

$$J = K_I = \sqrt{JE} \tag{3.20}$$

With E the Youngs modulus. For mixed mode loading, an interaction integral method is used to find the SIFs. As explained in section 2.4.2, the J integral is calculated for multiple auxiliary stress fields. This leads to a system of equations, which is able to solve for the stress intensity factors. The Abaqus documentation [50] gives a complete overview of this method.

The SIFs for a crack front are calculated in Abaqus for each element the crack face goes through. In Figure 3.12 a closeup of a crack formation for a certain simulation is shown. Only the part of the crack going through the rail material is taken into account. For this crack there are 14 elements crossed and thus 14 points where the SIFs are obtained. These points are shown in Figure 3.13. By default, for an even number of points, the point with index $x/2$ is chosen, for an odd number $x/2 + 0.5$. This point is assumed to be the middle of the crack tip where most crack growth is expected. The SIF values from this middle point are taken as input to calculate the growth rates.
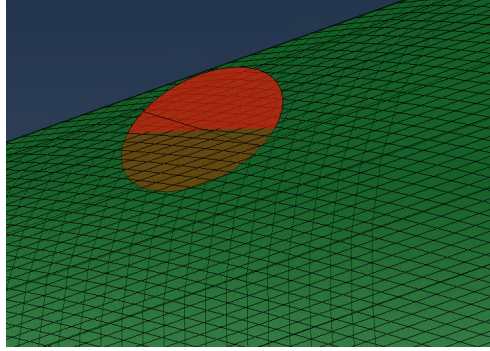
Figure 3.12: *close-up of crack with meshed rail.*
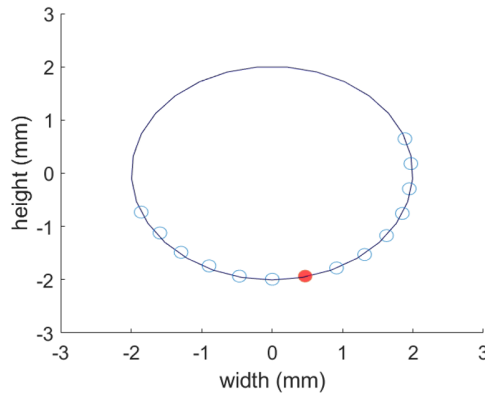
Figure 3.13: *Obtained SIF locations and used location (red).*

3.3.5 Matlab Growth Rate

Once the stress intensity factors are calculated, these have to be translated to a growth rate in order to obtain the damage index. From the Abaqus results, a datafile with obtained SIFs for each timestep is gathered. Abaqus calculates these SIFs for each element on which the crack front is running. Depending on the crack and mesh size, the number of obtained points can thus change. In all simulations, the point most in the middle of the crack is used for calculation of the growth rate.

In order to calculate the growth rate per cycle, the modified Paris law as used by Rodriguez et al. [40] is employed,

$$\frac{da}{dN} = 0.000507(\Delta K_{eq}^{3.74} - \Delta K_{th}^{3.74}) \tag{3.21}$$

with,

$$\Delta K_{eq} = \sqrt{\Delta K_I^2 + \left[\left(\frac{614}{507} \right) \cdot \Delta K_{II}^{3.21} \right]^{\frac{2}{3.74}}} \tag{3.22}$$

In these, the constants are from literature [51]. ΔK_{th} is an intrinsic threshold value of $4\,\mathrm{MPa}\sqrt{\mathrm{m}}$ according to Bogdanski et al. [52]. As crack opening and in-plane shear are assumed to be the most prominent modes, only these are taken into consideration for calculating the crack growth.

In the end, the crack growth and changing growth rate is analysed. As the Abaqus model only calculates SIFs for static cracks, changing crack growth rate is difficult to include. Another way has to be found to analyse growth rate. Two approaches were used to show this changing growth. For the first approach, a number of simulations were chosen and an elliptical crack of 1 mm was taken as initial crack. By running the model for these simulations, the SIFs for these were obtained. After that, the crack size was manually increased with either 0.5 mm or 0.25 mm. With this new setup, the model was run again to obtain the new SIFs and corresponding growth rates. This was done until a 10 mm crack size was reached. In this way the growth rate depending on the crack size could be determined. For the other approach, it was tried to get an idea of crack growth and how its geometry changes. For this, an initial simulation with a predefined 1 mm elliptical crack was used. Instead of manually increasing the crack size, the SIFs were taken after each simulation at the bottom of the crack and at the side of the crack. From this, the crack growth rate at the tip and the side could be calculated for that cycle. Then the assumption was made that for 10000 cycles this growth rate would be fixed. Using the growth rate, the crack size after these 10000 cycles could be calculated. From this, an updated crack geometry was obtained and placed in the model again. The model was then run with the updated crack size again. This cycle was done several times to see how the geometry of the crack changes and how the length and width of the crack act upon each other. As this was a time consuming analysis, only limited data is collected.

3.3.6 Damage Index

The final step for finding the needed data for the WLRM is to get a damage index from the growth rate. The damage index is defined as the inverse of the number of cycles to failure, $DI = 1/N_c$. The number of cycles after which critical crack length is reached (N_c), is approximately 10 mm according to Burstow [4]. Next to that, the assumption is made that growth rate is constant. The growth rate is calculated for one crack length in the previous steps. For calculations it is presumed that this stays constant until 10 mm crack length is reached. This will however be tested by running simulations with increasing crack sizes to measure change of growth rated. The critical crack length (10mm) is divided by growth rate in order to find the number of cycles to failure N_c. From this the Damage index is obtained and filled in into the WLRM curves.

3.3.7 Wear number

To be able to construct the x-axis of the WLRM, also the wear number has to be calculated. This can be done relatively easily. The wear number is defined as

$$T\gamma = T_x\gamma_x + T_y\gamma_y \tag{3.23}$$

The tangential and shear forces T_x, T_y can be described by the shear forces F_x, F_y found in Equation (3.4). The spin creepage is included in these equations. The longitudinal, lateral and spin creepages (relative velocity between wheel and rail normalized by the rolling velocity) can be obtained from the VI-Rail simulation data.

3.4 Numerical Experiments

Once the model is built, each step is tested and the Abaqus model is validated against earlier research, the objective is to reconstruct an RCF function with this model. This will be done in a few steps. First, from VI-Rail simulations already performed, a selection will be taken which will be fed into the designed model in order to get points in the WLRM graph. In two different manners, it is tried to get points which follow the line. For the first approach, only the coefficient of friction and the wear number obtained directly from VI-Rail are taken as simulation boundaries. As the coefficient of friction is assumed to be one of the most influential parameters, this value is kept at a constant of 0.43 for all researched simulations. This is done as Burstow obtained similar friction coefficients. This boundary was used to filter VI-Rail simulations from which 45 were taken to try and form the WLRM line. These points are shown in blue in Figure 3.14. It proved that this approach led to many points far from the Burstow line. To reduce the offset, another approach is tried.
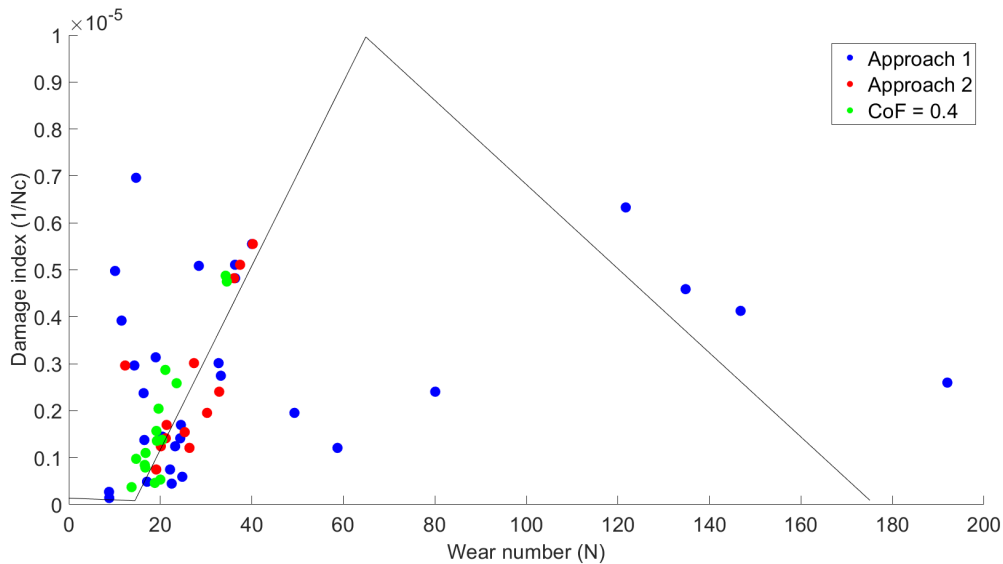
Figure 3.14: *Simulation results of both approaches and simulations with $\mu = 0.4$.*

The possible reason for the high number of offsets could be the low similarity of the used simulations with the field data from Burstow. Therefore, the input parameters of Burstow are analysed and compared to the simulations parameters.

By studying the parameters of Burstows field results, simulations with more similarities can be filtered. In Burstows work [1], five main force and contact patch parameters are shown which can be compared for the different test results. An overview of the field results of Burstows work can be found in Appendix A. The wear number, the shear force, contact stress, shear force coefficient and the contact patch area are analysed. Table 3.2 shows these load parameters and their ranges. Finally, only simulations with wear numbers between 15 and 65 N were taken as this is the range in which RCF is dominant.

Table 3.2: *Load parameter boundaries.*

Parameter	Wear number	Vector Sum Shear Force	Contact Stress	Shear Force Coefficient	Contact Patch Area
Variable	$T_\gamma = T_x\gamma_x + T_y\gamma_y$	$F_s = \sqrt{T_x^2 + T_y^2}$	$P_m = \frac{3Fn}{2\pi ab}$	$\mu = \frac{T_x}{Fn}$	$A = \pi ab$
Range	15 - 65 N	10 - 20 kN	600 - 1500 MPa	0.1 - 0.45	40 - 110 mm^2

For the second approach, the simulations performed for the first approach are filtered, such that only the ones with load parameters within the given boundaries remain. Apart from that, the wear number is not taken directly from VI-Rail results anymore, but is calculated as described in Section 3.3.7. This is done as there sometimes is a significant difference between the calculated wear number and the one found in VI-Rail. Because VI-Rail does not take into account spin, these differences in wear numbers are mainly seen when spin is larger. With this different approach, the number of points that can be compared to Burstow decreases significantly. Nevertheless, points closer to the Burstow RCF line are obtained with this approach. Even though, there are still some outliers are present. In Figure 3.14 the red points show the results of using this approach.

Finally, the second approach is once more repeated for another set of simulations, this time with the coefficient of friction being 0.4. As this is still in the range of the Burstow results, similar points were expected and obtained. The wear numbers were calculated again. The results are shown in Figure 3.14 as the green points. These points are found to have only little offset with the Burstow line.

Once it is shown that the RCF model is able to deliver results similar to Burstows field results, the model is used to show the influence of different parameters on the RCF function. Meghoe [53] identified 8 parameters having significant influence on rail wear. These parameters are chosen to be operational condition parameters, parameters easily obtainable from real cases. As Meghoe has performed VI-Rail simulations with these parameters, these are used again for this thesis. In Table 3.3 an overview of these parameters and their ranges is given. It is assumed that these parameters not only have a significant impact on wear, but also on RCF. It will be analysed if these really have an impact on the RCF model.

Table 3.3: *Input Parameters and ranges.*

Parameter	Symbol	Unit	Range	Base Value
Vertical wear depth	h	mm	0 - 12.5	6
Curve Radius	R	m	1400 - 2600	2000
Rail cant	E_a	mm	70 - 130	100
Coefficient of friction	μ	-	0.28 - 0.52	0.4
Vehicle speed	V	m/s	23.33 - 43.33	33.33
Longitudinal stiffness (primary suspension)	k_x	N/m	$4.32 * 10^5 - 8.00 * 10^5$	$6.17 * 10^5$
Lateral stiffness (primary suspension)	k_y	N/m	$4.32 * 10^5 - 8.00 * 10^5$	$6.17 * 10^5$
Axle load	m	N	22400 -41600	30000

To analyse the influence of these parameters on the RCF curve, multiple existing simulations with input parameters in the defined ranges are taken and the point on the WLRM is determined with the model. After that, the input parameters are changed one after another to find points on the WLRM for variable parameters. By doing this

for enough simulations, trends should be found in the movement of points based on parameter changes. It is expected that the slope of the RCF curve will change based on the parameter changes. The magnitude of this change will indicate the parameter influence.

To find a final RCF function, the idea is to set up a meta-model which is described using the points found in the WLRM with the different parameters. To do this, a quadratic regression formula based on Response Surface Methodology is used [54]. This methodology is based on data fitting on either a linear or quadratic function, using regression techniques. Meghoe [53] proved the quadratic formula for this theory to be valid for the wear function of the WLRM. For RCF, the same parameters except material hardness were used. as only one material was analysed, hardness was not included. Because of these similarities with the wear function, it is also tried to fit an RCF function using this quadratic formula. This quadratic formula is described as:

$$y(x) = \beta_0 + \sum_{i=1}^{k} \beta_i x_i + \sum_{i=1}^{k} \epsilon_i x_i^2 + \sum_{i=1}^{k-1} \sum_{j>i}^{k} \zeta_{ij} x_i x_j \tag{3.24}$$

This equation is built with the idea that a certain model contains k input variables. The ith input variable is denoted as x_i with regression estimations β_i, ϵ_i and ζ_{ij} for that variable. The last term in the equation is there to cover the correlation between the different variables. In order to estimate the coefficients in this equation, the number of simulations n must satisfy $n \geq k + k + \binom{k}{2} + 1$ [54]. In this case, where 8 input parameters are used, at least 45 simulations are needed. These parameters are chosen as an One-Factor-At-a–Time (OFAT) analysis was performed by Meghoe [53] to find the most influential parameters on wear damage on rails. These eight were found to be most significant. Because of this, it was decided to cover fatigue with the same parameters. To be covered, at least 300 simulations are run to find these estimates and set up a function to declare the RCF propagation phase. Before this function really could be used, it is validated by comparing the Damage Index output of the equation with the Damage Index output from the FEM model.

4 | Results and Discussion

In the methodology a framework was set up to find the damage Index and wear number for different rail situations. By using the right parameter settings, results similar to Burstow could be obtained. In this section, the parameters influencing the Damage Index and wear number are further analysed. It will be studied how the parameters in Table 3.3 change the RCF WLRM line. Two approaches are tried to visualise the influence of these parameters. Eventually, a regression function is set up that is used to plot the parameter influence on the Damage Index. Finally, a test case is set up to see if an RCF function could be constructed for a specific rail situation. In the end, it is tried to show if a straight RCF line could be drawn for a specific case.

4.1 Parameter influence

The RCF damage function depends on different track situations. The influence of operational input parameters is analysed to see how the function changes. The input parameters introduced in Table 3.3 are used for this. Existing VI-Rail simulations are taken as a starting point. For four of the parameters, there are 10-20 simulations that are used. In these simulations, the analysed parameter is kept at a fixed value, while the other parameters are variable for the different simulations. For the selected simulations, the Damage Index and wear number were obtained. The results are shown in Figure 4.1. When the coefficient of friction is constant (0.4), the points are close to the Burstow line. With only speed or mass being fixed, the results do not coincide with the existing line. There is no clear trend for these points. Because 7 parameters are variable, one cannot say which parameter(s) exactly cause this randomness. Furthermore, the points for friction coefficient and radius are overlapping for all cases. In the data, it was found that in the fixed radius simulations, the coefficient of friction was also kept constant. It can be seen that it does not matter if the radius is constant or variable, as both give similar results (green and black points). As the black and green points are on the same spots, and are almost similar, the black points are less visible.
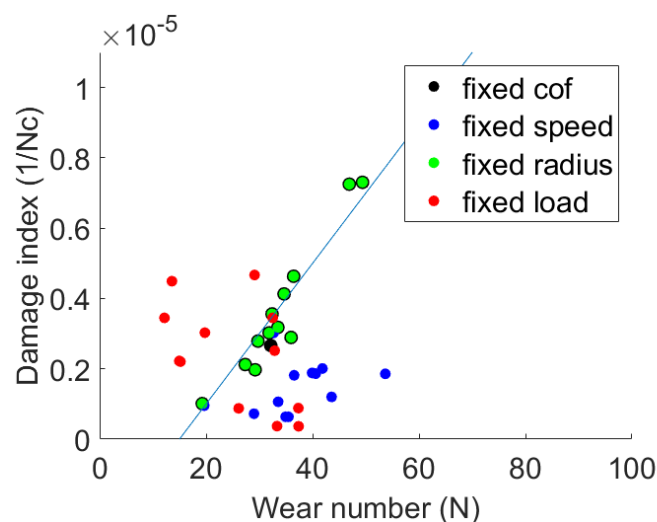

Figure 4.1: *Simulations with one fixed input parameter.*

Because Figure Figure 4.1 does not show clear trends in the parameter influence, another approach was used. To get a more precise idea of the influence of each input parameter independently, only one parameter should be variable while the others stay constant. VI-Rail simulations for this approach were performed for this study. Multiple simulations from an existing batch were taken as original simulations. From these simulations, the input parameters were, one-by-one, changed to the minimum value, the maximum value and a value in the middle of the range (values in Table 3.3). The damage Indices and wear numbers were determined using the set-up framework, with the XFEM model and wear number calculated from own results. To get a clear view of the changes on the RCF function, 3 original simulations were taken as input. These three simulations were chosen as their point in the WLRM was lying on or close to the original RCF function. In Figures 4.2 to 4.9 the results are shown. In each of these graphs, each simulation has its own shape and colour. The star in the corresponding colour shows the original simulation. The size of the shape determines the size of the analysed parameter. Referring back to Table 3.3, the small shape is for the minimum value, the middle shape for the base value and the large shape is for the maximum value. The orange dotted line is drawn into the graph to show how the function changes based on the changing parameter. The black arrow shows the direction in which the RCF function changes if the analysed parameter increases.

Figure 4.2 shows the influence of rail cant on the wear number and Damage Index. For all simulations, a clear increase in wear number can be seen when the cant is increased. By tracing the wear number back to Equation (3.23), the wear number can be changed by a variation in either creep force or creepage. For increasing rail cant, generally the longitudinal creepage, perpendicular to the rail, is increased. Apart from the maximum point of the black simulation, the Damage Index decreases slightly for increasing cant. Due to the increased cant, the stresses in the crack tip are decreased, which explains the decreased Damage Index. The points of these simulations seem to show that the RCF function would not change in slope, but it would move sideways depending on cant changes.
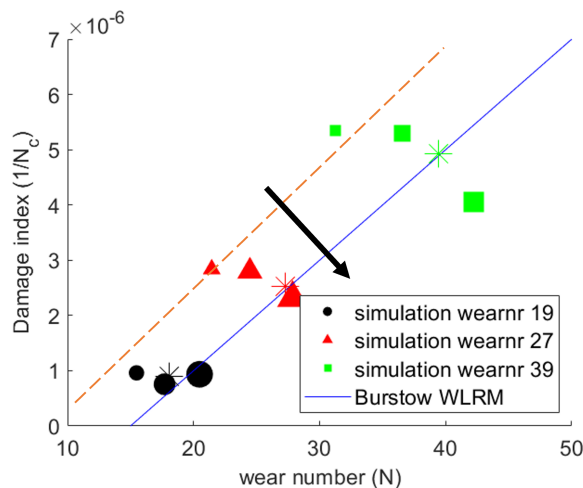
Figure 4.2: *Simulations with variable rail cant.*

For the coefficient of friction, Figure 4.3 shows the results. All simulations show a slight decrease in wear number for increasing COF. As more friction generally gives higher wear rates and thus a higher wear number, this result was not expected. The simulation data showed that, due to the increased friction, the creepage is decreased. There is less slip between the wheel and the rail, which decreases the wear number.

The Damage Index is increased, as the shear stresses in the contact area are larger for larger friction. Although the trend is not the most clear, the expectation is made that, for increasing COF, the slope of the RCF function increases. The black simulation is less clear in showing this. Because the black simulation is relatively low in the graph and therefore less distinctive, the trend could be less clear.
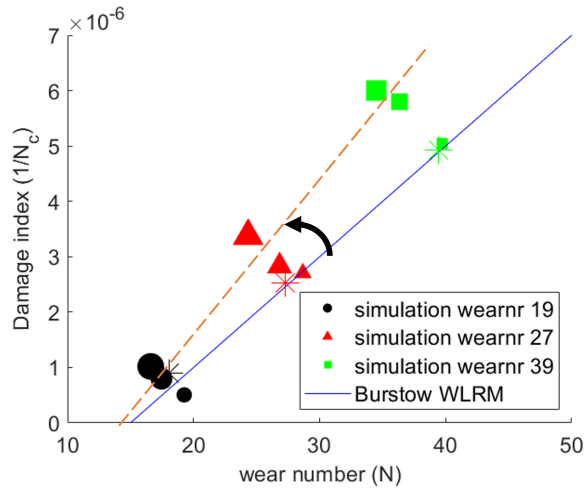

Figure 4.3: *Simulations with variable coefficient of friction.*

In Figure 4.4 the changes due to curve radius variation are shown. All simulations clearly show a significant decrease in wear number for increasing curve radius. The Damage Index however stays constant. The creepage parallel to the rail decreases for increasing curve radii, causing a decreasing wear number. As cracks mainly form in curves [3], it was expected that the Damage Index would also decrease if the curve radius was increased. This is however not the case. The SIFs in the crack tip stay reasonably similar. With sharper curves, the shear stresses are a bit lower, but these results show that this small decrease has no significant effect on the Damage Index. In the WLRM, the RCF function seems to increase the slope and moves to the right for increasing radii.
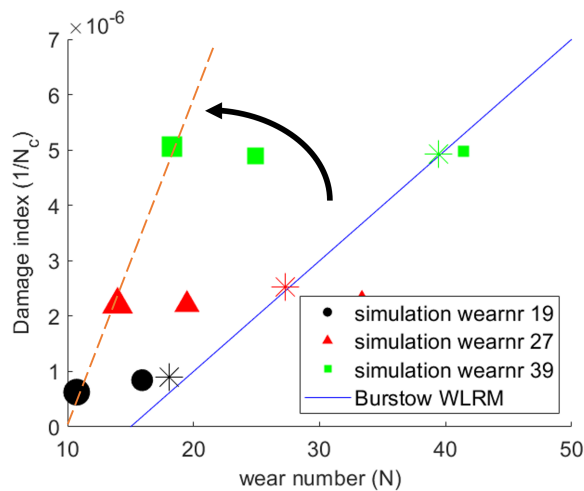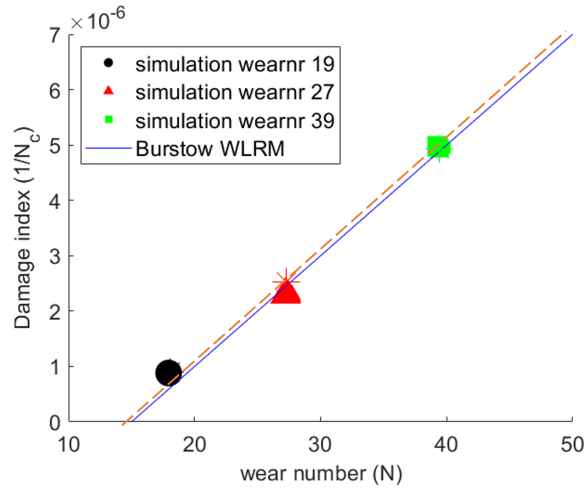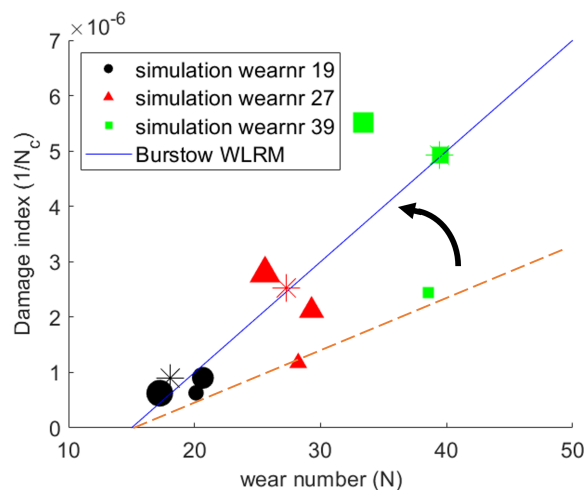

Figure 4.4: *Simulations with variable curvature.*

The lateral stiffness shown in Figure 4.5 shows to have very little impact on the placement of the simulation results on the WLRM. From these results, it seems that lateral stiffness does not contribute significantly to the wear number or Damage Index. The RCF function does not change significantly from different lateral stiffness.

Figure 4.5: *Simulations with variable lateral stiffness.*

In Figure 4.6 The axle load variation is shown. The wear number for this parameter seems to stay relatively stable for smaller loads but for larger loads, the wear number will decrease. With heavier loads, more wear would be expected and thus a higher wear number. Nevertheless, Due to the heavier loads, there is less slip and thus the creepage is decreased. This causes the wear number to decrease. The Damage Index is increased for higher loads. This is expected as higher loads cause higher stresses and thus larger SIFs. These points in the graph show that the slope of the RCF curve would change for changing loads.

Figure 4.6: *Simulations with variable axle load.*

The influence of longitudinal stiffness on the simulation results can be seen in Figure 4.7. The damage index is not influenced significantly by changing the longi-

tudinal stiffness. The wear number slightly increases with higher stiffness. As the stiffness is higher, the tangential shear force is increased slightly. This change will increase the wear number. Because of this, a small movement of the RCF function is expected from changing the longitudinal stiffness.
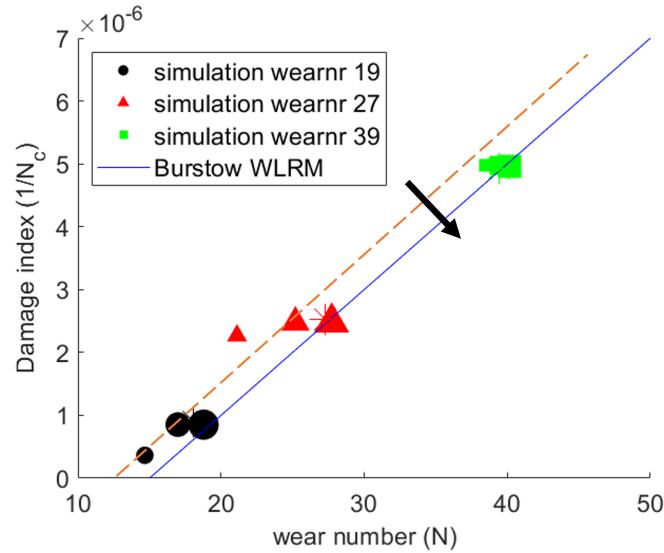
Figure 4.7: *Simulations with variable longitudinal stiffness.*

Figure 4.8 shows the influence of speed. With increasing speed, the wear number decreases significantly whereas the Damage Index stays almost constant. The increased speed causes a decrease in slip and thus the creepages are lower. This explains the decreasing wear number. As expected, increased speeds would cause more damage. For the simulations with the higher wear number, it can be seen that the Damage Index is indeed increased. For the simulations with a lower wear number, this increase is less visible. For increasing speed, The RCF curve moves and changes the slope according to these results.
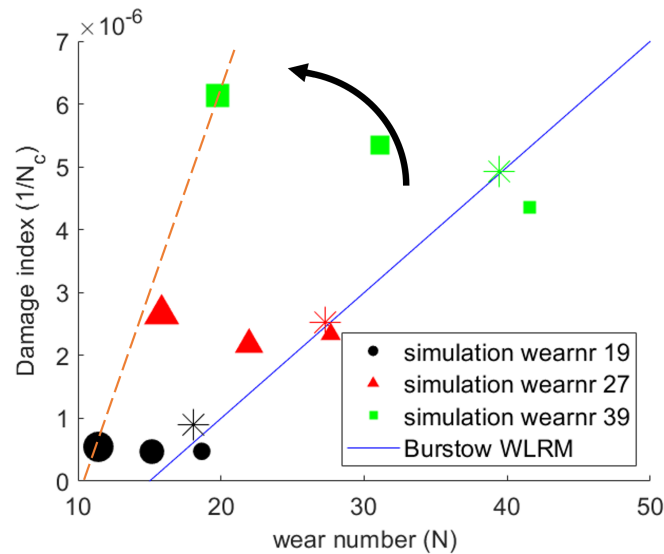
Figure 4.8: *Simulations with variable train speed.*

Finally, in Figure 4.9 the influence of the vertical wear depth is shown. The minimal value is not visible as these are too high to be in the scope of the plot. The wear number for changing vertical wear depth does decrease a little for increasing depth. A small decrease in creepage is the cause for this; there is less slip. The Damage Index significantly decreases for increasing vertical wear depth. When the wear depth is 0, crack growth is the main contributor to failure. Cracks grow faster in that case and the Damage Index is higher. If the wear depth is high, cracks have no physical place to grow and the Damage Index for RCF is low. Because of this, the expected change in the RFC curve is a lower slope for higher wear depths.
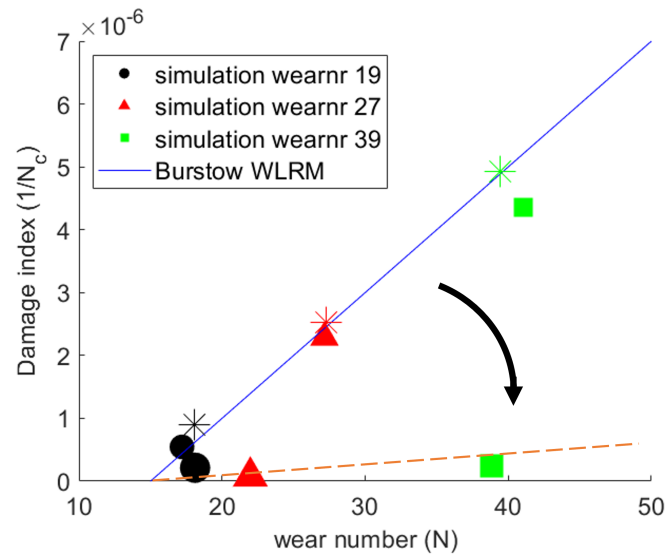

Figure 4.9: *Simulations with variable vertical wear depth.*

Important to see from these graphs is that for the most influential parameters, the RCF line is either moved along the x-axis or rotated around the fatigue threshold value. When the line is rotated, the fatigue threshold value stays constant. In this case, the number of cycles until fatigue cracks appear does not change. Depending on the direction of the rotation, the Damage Index is either increased or decreased. For clockwise rotations, The Damage Index generally gets lower for cases with similar wear numbers. It would thus take more cycles until critical crack lengths are obtained. Anti-clockwise rotation would result in higher Damage Indices and faster crack growth. Instead of rotating the line, it can also be moved along the x-axis of the graph. This would change the fatigue threshold value. If the line is moved to the right, the fatigue threshold is increased. The wear number, and thus the creep force or creepage, needs to be higher to form cracks. Despite this movement, the slope of the line would not change. This means that for cases with similar wear numbers, the Damage Indices would be smaller. The number of cycles until critical crack length would be larger. In Figure 4.10 an example is given for a rotating and a moving RCF function. For a fictional case with a wear number of 30 N, the damage Index would be higher for anti-clockwise rotation and negative movement. For clockwise rotations and positive movement, the Damage Index would decrease.
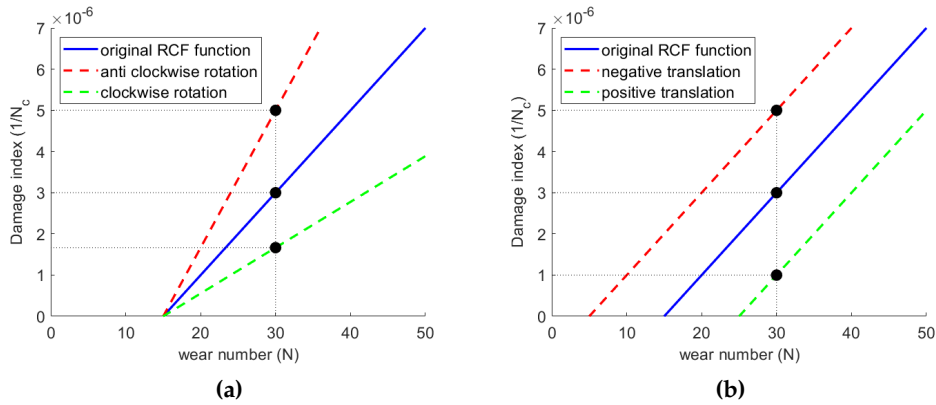
Figure 4.10: *Example rotation and translation of RCF function.*

4.2 Regression Function

The previous results have shown the estimated influence of the different input parameters. These results are used to set up a regression formula from Equation (3.24). This formula could be used to quickly find a Damage Index for a certain case without having to run the complete framework from Figure 3.6. The three simulations analysed in the last section did not generate enough results to train the formula appropriately, as a minimum of 45 results are needed. Multiple other simulations were used to overcome this shortcoming. 15 random simulations were taken and their parameters were changed in the same way as shown in Section 4.1. In total, 375 results were found and used to form the regression formula. In Equation (3.24), x is given by the input parameters and their variation. The output of the system y is given by the damage indices. As the parameters and the Damage Indices are known, a system of equations could be set up. This system of equations could then be used to find the regression estimators β, ϵ and ζ.

To test if the set-up formula actually can predict the Damage Index for a random situation, a validation test was done. Fifteen random simulations were taken, which were not used as input for the regression formula. The Damage Indices of these simulations were determined using the XFEM model and the regression formula. In Figure 4.11 the comparison between both is shown. Even though the formula is not able to predict the Damage Indices precisely, the error is always below 20% of the FEM model value. Figure 4.12 shows the Damage Index found by the FEM model and the Damage Index found by the formula. 15 Simulations are used to show this comparison. The graph shows that for lower Damage Indices the error is low. For higher values, the error can be larger. By studying the input data, it was seen that if the vertical wear depth is at the end of the range ($h \leq 2\text{mm}, h \geq 10\text{mm}$), then the error is generally larger. For cases with the vertical wear depth between 2 and 10 mm the error is often below 10%.

Using the regression formula, it was possible to create graphs with the Damage Index as a function of the variable parameter. These graphs show the influence of the specific parameter on the Damage Index. To create these graphs, all parameters were set at their base values, and only the analysed parameter was varied between the minimum and maximum values. Figure 4.13 shows an overview of these results. In the graphs, the Damage Index is set up against the parameter. In theory, the plot in these graphs should show similar trends to those already shown in the previous chapter. For example, the rail cant, the graph shows, just as Figure 4.2, that for increasing cant, the Damage Index decreases. The longitudinal stiffness shows
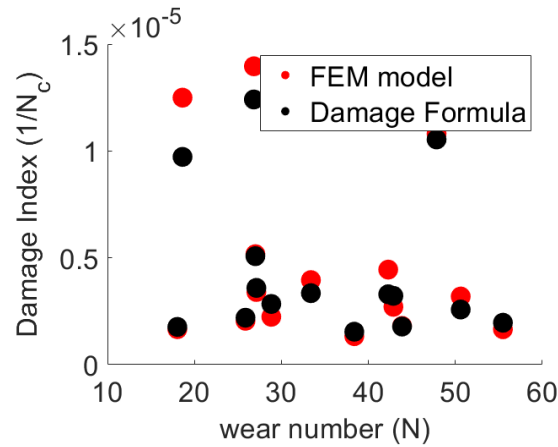
Figure 4.11: *Comparison between 2 approaches to obtain the Damage Index.*
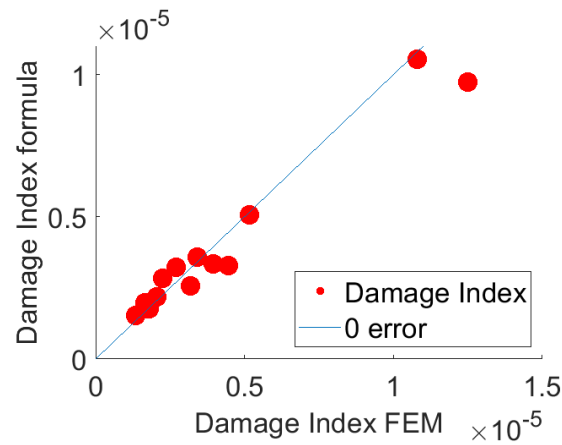
Figure 4.12: *Comparison between Damage Indices.*

that there is only little change in the Damage Index for increasing stiffness. Some graphs also show the parameter influence in more detail. In Figure 4.4, the Damage Index remains constant for increasing curve radii. The graph of Figure 4.13c however shows that the damage index does increase a bit for increasing radii. Finally, most of the parameters seem to have a (almost) linear relationship with the increase of the parameter and the change in the Damage Index. The vertical wear depth does show more quadratic behaviour. From Figure 4.9 it was expected that the line would only decrease for increasing wear depth, but the formula shows that after a certain value, the Damage Index actually will increase. For most parameters, the expected results are found and thus the formula is expected to be correct for those parameters. The vertical wear depth shows non-linear results and has large estimator sizes. It could be the case that the vertical wear depth cannot as easily be explained with this regression formula. This is however not researched in further detail.
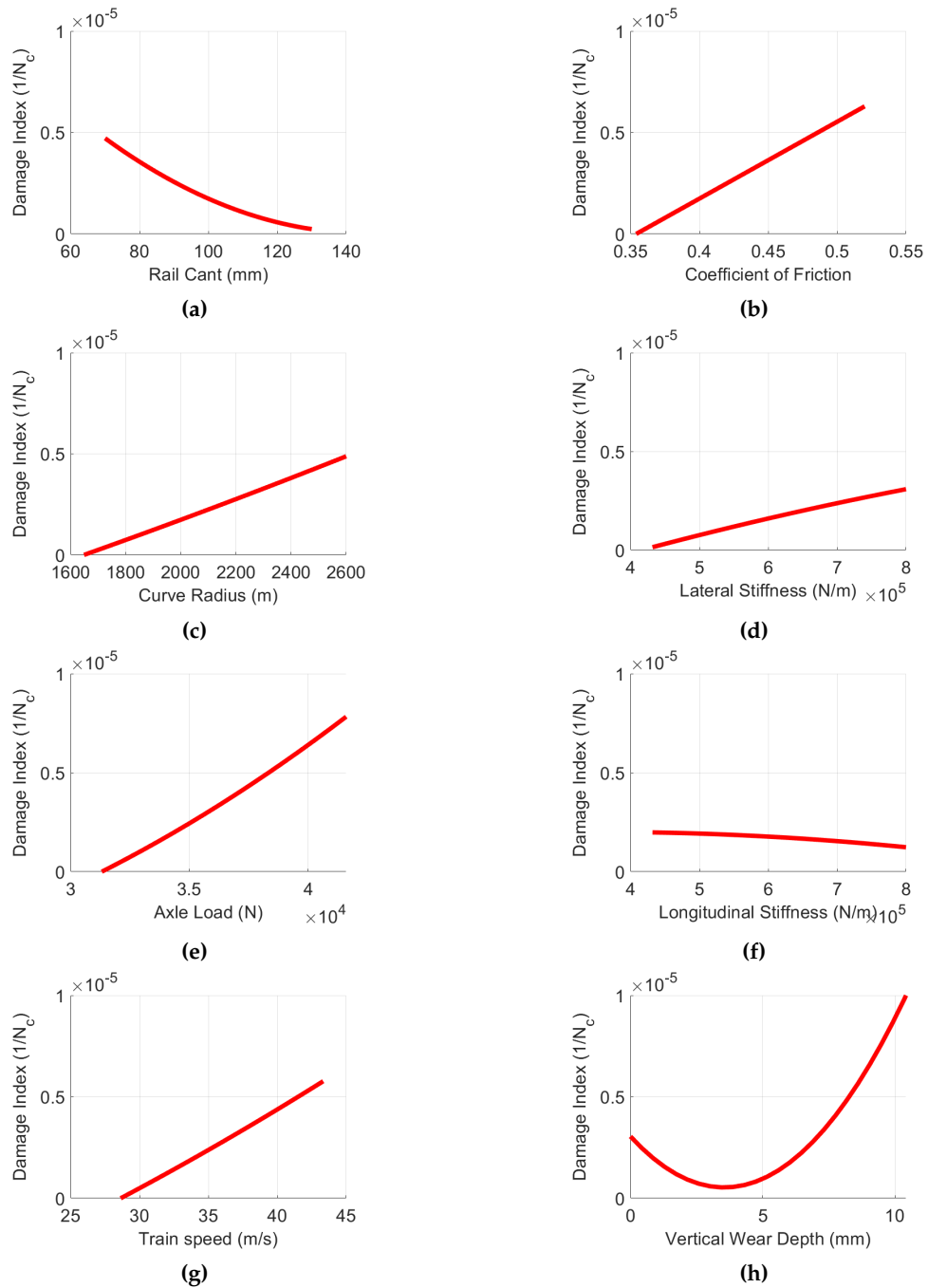
Figure 4.13: *Parameter influence based on regression formula.*

The last thing to pay attention to is the β, ϵ and ζ estimators of the function. Especially their sizes can show some information. If the estimator is large, it is expected that the (combination of) parameters associated with that estimator have a large influence on the Damage Index. For the β estimators combined with only one parameter (second term in Equation (3.24), linear relation) there are relatively high estimators for the radius, cant, speed and vertical wear depth. The coefficient of friction has a very low estimator. Also, both stiffnesses have little linear relation. These parameters seem to be less influential when looking at individual parameters. Similar results are obtained for the squared parameters (ϵ). However, the estimators for the squared parameters are generally lower than the single parameters. In Figure 4.14 the linear and quadratic estimators are shown. The bar graph of Figure 4.15 shows the estimator size for combinations of two parameters (ζ estimator). It can be seen that the vertical wear depth in combination with all other parameters is an important factor. The Coefficient of friction with radius, cant and speed also has higher values. The stiffnesses seem rather unimportant also in this graph.

Figure 4.14: *Estimator size for all single parameters.*

Figure 4.15: *Estimator size for all parameter combinations.*

4.3   RCF function development
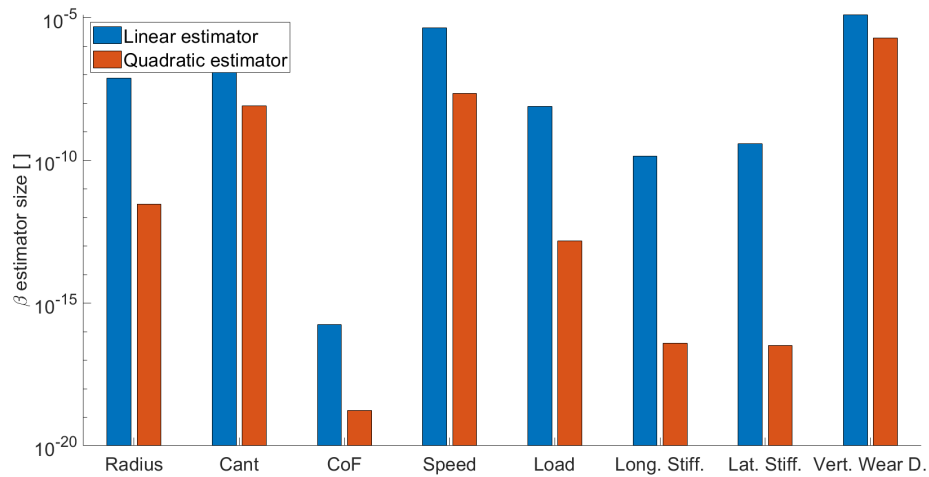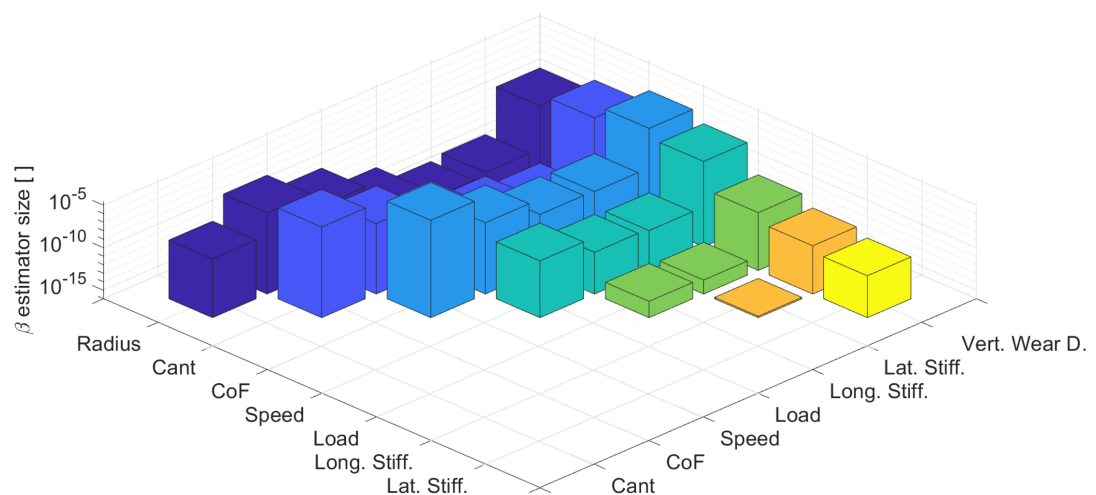
By using the regression formula, a simplified method is found to determine the Damage Index. After showing the influence of different parameters, it should be possible to create RCF functions for various situations. The difficulty in this is finding a clear relation between the points on the RCF WLRM line. As each result only presents one point in the wear number / Damage Index graph, drawing a line is only possible if multiple points can be found that can be related to each other. A test case is set up to try to find an RCF line for a specific situation. In this theoretical case a rail with a fixed radius, cant and vertical wear depth is used. In an ideal situation, the analysed rail is used by only one train type. Because this is not often the case, for this theoretical problem, the rail is primarily used by four different types of trains, all with different axle loads and stiffnesses. Train 1 has the highest axle load. This decreases to the lowest axle load for train 4. The longitudinal and lateral stiffness are assumed to be the same for a train. The size of these stiffnesses however is changed for each train. The Coefficient of Friction is varied between 0.3 and 0.5 for these train types. Finally, a speed of 140 km/h and a speed of 100 km/h are used as the standard speeds with which the trains travel. Using these parameters, The Damage Indexes and wear numbers of multiple of these cases were obtained. In Figure 4.16 these results are shown. The colour of the symbol indicates the train used, the circle and triangle indicate if 100 or 140 km/h is used respectively, and the size of the symbol indicates if $\mu = 0.3$, $\mu = 0.4$ or $\mu = 0.5$. The parameters for all trains are given in Table 4.1

Table 4.1: *Test case parameters.*

	Train 1	Train 2	Train 3	Train 4
Vertical wear depth	6 mm	6 mm	6 mm	6 mm
Curve Radius	1500 m	1500 m	1500 m	1500 m
Rail cant	120 mm	120 mm	120 mm	120 mm
Coefficient of friction	0.3-0.5	0.3-0.5	0.3-0.5	0.3-0.5
Vehicle speed	100-140 km/h	100-140 km/h	100-140 km/h	100-140 km/h
Longitudinal stiffness	6*10^5 N/m	7*10^5 N/m	5*10^5 N/m	8*10^5 N/m
Lateral Stiffness	6*10^5 N/m	7*10^5 N/m	5*10^5 N/m	8*10^5 N/m
Axle load	37700	37000	36500	29400

In an ideal situation, the points in the graph shown would be lying on a line, making it easy to create the RCF function for the specific test case. As has been shown before however, the different parameters have influence on the Damage Index. In reality, the points form a cloud from which it is difficult to draw a solution. One does see the influence of the parameters as explained before. For example, train 4 (blue) has three points on the right of the graph. with increasing COF the wear number decreases, as is also shown in Figure 4.3. The most right point has $\mu = 0.3$ while the left point has $\mu = 0.5$. The other points of train 4 are performed with a higher speed. Just as shown before, an increase in speed significantly decreases the wear number. For higher speeds, the simulations show to be less influenced by the COF. Therefore, an RCF line could be drawn through these points. At lower speed, the COF has more influence, the points of the loads are farther from each other. As shown in Figure 4.15 the combination speed and the COF has a relatively high estimator, making them significantly dependent on each other. This explains why the COF is more influential at lower speed. Drawing an RCF curve for these points is therefore more difficult. One could suggest to give a range in which the RCF curve falls, but a founded estimation of the RCF function placement is not possible with only these points.
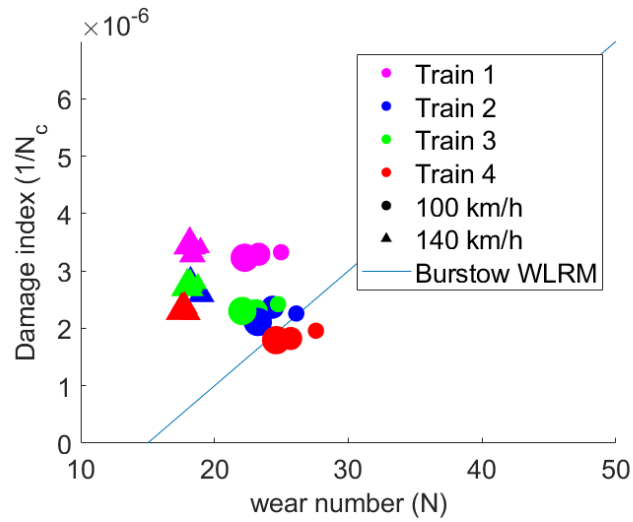
Figure 4.16: *WLRM for test case with four train types.*

As it is shown to be difficult to obtain an RCF function for a specific rail location, it can be argued if it is useful to draw an RCF function for a specific situation. If these clouds of points are not able to comprehensively show how the RCF function should behave, it is inconvenient to draw such a line. Next to that, it could be questioned what the obtained line exactly would explain. The simulated cases will give points on the line for which that line is valid, but it cannot be said without hesitation that other cases will also be on that line. It could be discussed that the only real added value of the RCF curve is that this will show if and when the RCF dominant phase starts and when wear will influence the rail Damage. Therefore it is suggested to omit creating the WLRM and instead look at the Damage Index for specific situations only. As it is relatively easy to find the Damage Index and wear number for a case, this would be a straightforward approach to predict failure and maintenance needs. The only difficulty in using only points is that the dominant failure mechanism (wear or RCF) is not immediately clear. The Damage Index for both mechanisms should be found to compare and determine the dominant mechanism. The number of cycles to failure can then be predicted based on the dominant mechanism.
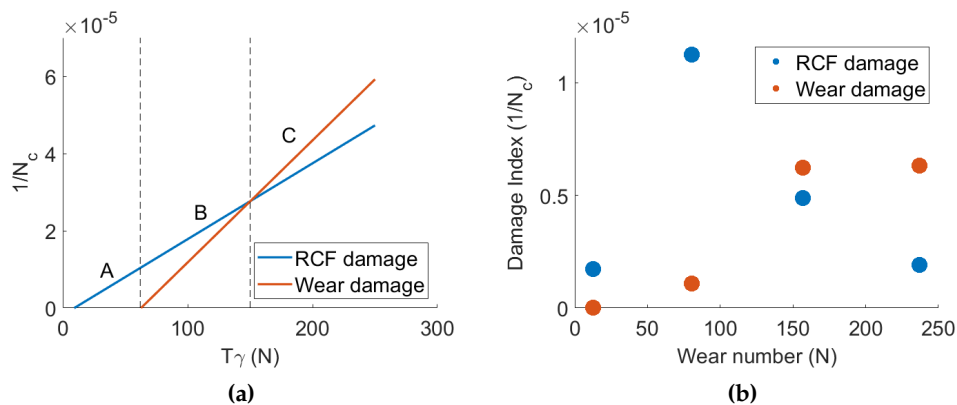

Figure 4.17: *RCF function and Wear function Damage comparison.*

To be able to compare both mechanisms and determine the dominant one, some theory of the WLRM stays relevant. In Figure 4.17a the basis of the WLRM is shown again. There are three important distinctive regions. In region A, there is only fatigue and thus this is the dominant mechanism. In region B there is also some influence from wear, but fatigue is still dominant. In region C, the wear has become dominant, the rail wears away too fast to form fatigue cracks. If it is assumed that these specific regions still hold, the wear and fatigue damage can easily be compared to find the dominant mechanism. In Figure 4.17b these two damages are compared. The RCF damage is calculated using the quadratic regression formula derived in this thesis. The wear damage is calculated using a similar equation to calculate the wear rate [53]. Four random simulations are taken which show the different phases clearly. The first simulation, with a wear number of approximately 15 N, there is some RCF damage. As the wear damage has a value of 0, there is no wear taking place. The damage would thus be in phase A and only RCF would be of influence. For the second simulation (wear number of 80 N), both the wear and RCF are above 0. As the RCF damage is still higher than the wear, there is still crack formation happening, despite wear also taking place. This simulation can be placed in phase B. Both the wear and the RCF are of importance. In simulation 3, wear number of 160 N, both damages are almost the same, with the wear being slightly higher. This means that the intersection between both functions has just been passed and phase C has been reached. The wear is now dominant as fatigue cracks have no time to form. In the last simulation, wear number of 230 N, the wear has become even more dominant, so even further in phase C. The simulations were not compared with each other, random ones were chosen. Because of this, there is no linear correlation between the wear number increase and the damage index increase. Nevertheless, by identifying the wear and RCF damage for any condition, the dominant mechanism could easily be obtained and an estimation of the number of cycles until failure could be given.

4.4   Crack growth influence

One final aspect which should still be included in the model is that changing crack growth is not taken into account. In the XFEM model, the Stress Intensity Factors are calculated when the crack is one or two millimetres in length. The growth rate is calculated for this crack and assumed to be constant. The problem with this assumption is that the growth rate is not stable during the full lifetime of the rail. The crack develops and changes geometry. The stresses and thus the SIFs in the crack are changed by this. The Paris law (Figure 2.5), from which Equation (3.21) is a modification, shows that the growth rate generally increases with increasing SIFs. Test specimens from different research show that increased crack lengths cause increased Stress Intensity Factors and crack growth rates [55]. For this study, it was tried to analyse the effect of changing crack sizes. Three random simulations were taken, which were run through the XFEM model. An elliptical crack was used with an initial radius of 1 mm. After performing a run with the model, the growth rate for that crack was obtained after which the crack size was manually increased. For simulations 1 and 2, the crack size was increased by 0.5 mm. For simulation 3 (wear number 33.23 N), the crack size was increased by 0.25 mm. After the size increment, the simulation was run through the XFEM model again. These steps were repeated multiple times for each simulation until a crack size of 10 mm was reached. In Figure 4.18 the crack growth rate is set up against the crack length for these three simulations.
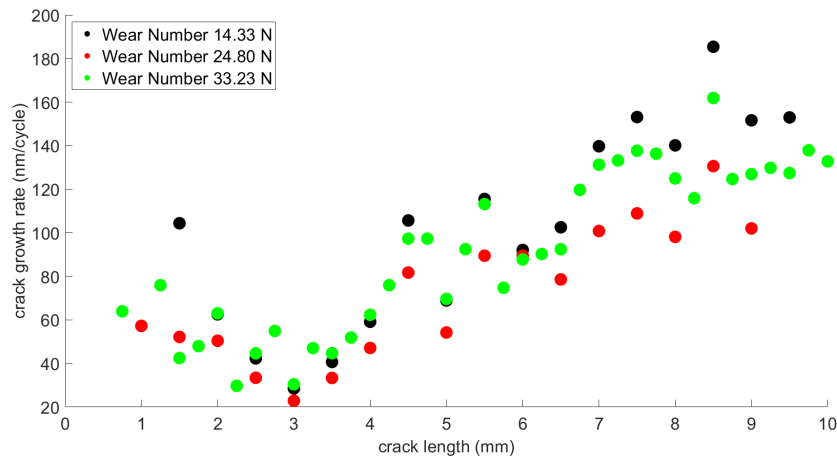
Figure 4.18: *Crack growth rate variation over crack length.*

The graph shows that after a 3 mm crack length, the growth rate increases almost in a linear manner. Before the 3 mm crack length, the growth rate seems to decrease. This is not expected and has partly to do with the model being less precise with smaller cracks. As the mesh is not small enough to capture the minimal crack, some problems could exist in getting stresses at the exact crack tip. Next to that, Burstow [4] shows in his crack growth predictions that the growth rate in certain situations stays almost constant at 1-3 mm. Another study by Trollé [56] about crack propagation in rails also shows the behaviour of decreasing crack growth rate before 3 mm crack length, whereafter the growth rate starts to increase again. Even though no reason for this is given, it is thus shown before.

In the crack growth rate, also the geometry of the crack plays a role. In the XFEM model, a semi-circular crack was used as the initial crack face. In 3D simulation, cracks are generally modelled as semi-elliptical cracks with a vertical axis a being the length of the crack and a horizontal axis b being the width of the crack. As explained before, for this study, only one load cycle is placed on the crack and no real crack growth takes place in the model. Therefore, in the XFEM model, the crack stays circular with a constant radius. In real life, however, a crack would never be a perfect semicircle. Because the model is 3D and the crack does not go fully through the rail, a rounded semi-elliptical crack face is the best approximation to a simple initiated crack. In this crack face, the stresses may be different at different locations. In Figure 3.13 it has been shown that the SIFs are obtained for multiple locations at the crack front. Only the middle node is taken for the Damage Index calculation, but the other nodes could have significantly different SIFs. This means that the elliptical crack could grow at different speeds in different locations. It could be chosen to look at both axes of the elliptical crack, a and b, as both can have different growth speeds. Figure 4.19 shows what happens with the crack size if both these axes are taken into account. To obtain these results, an initial crack with a size of 1 mm length and 1 mm width radius was situated on the rail for a random VI-Rail simulation. After each XFEM model run, the growth rate for the corresponding axis was determined by obtaining the SIFs at the crack tip and at the crack sides. It was then calculated what the length of the axes would be after 10000 cycles with that growth rate. That redefined length was placed in the XFEM model and a simulation was done again to find the new growth rates. These steps were repeated multiple times until an idea of the crack growth and the differences between both axes was gathered. As can be seen, the horizontal axis, the crack width, starts growing faster. Eventually, both the width and the length of the crack will grow at similar speed, but the width will be

significantly larger at that stage. Even though they have a similar rate at some times, the growth rates are different. It can thus not be said that the crack will remain circular during the full lifetime. This should be taken into consideration for Damage calculations, but was not done for this study.
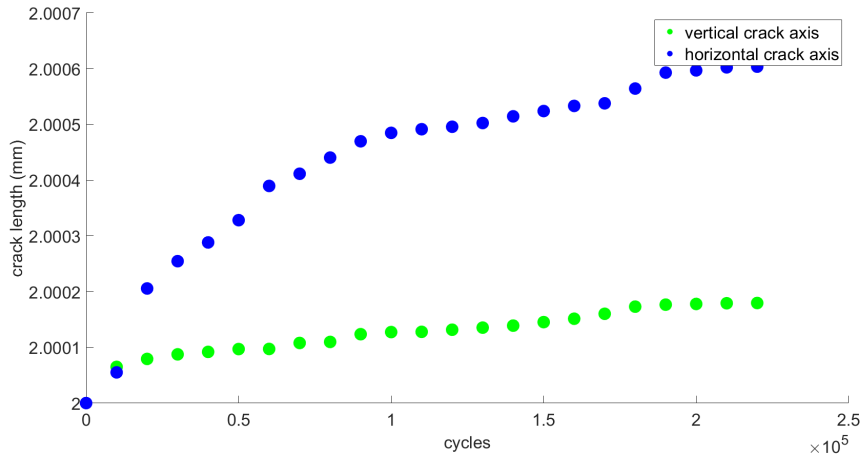

Figure 4.19: *Difference in growth of axes of crack.*

4.5   Discussion

Finally, some decisions and considerations have to be discussed in more depth. Most important in this is the lack of inclusion of the initiation phase. As explained in the Theoretical Framework (Chapter 2), crack growth has two distinctive phases; the initiation phase and the propagation phase. Both should be treated individually. Due to time constraints, only the propagation phase was analysed in this study.

Another point that has to be discussed is the geometry and the location of the crack on the rail. For this study, the crack was kept at an angle of 30°. This was chosen as the model by Rodriguez et al. [40] made use of the same angle, and this is a commonly found angle for Head Checking in rails. It was not tried to change the angle, but a change in results would be expected if this was done. Sung et al. [57] did look into this and showed that for steeper angles the growth rate generally decreased. If angles significantly different from 30°are found to be present for a specific case, the XFEM model should be changed to fit these different angles.

Finally regarding the crack, the location could be a point of interest. For this research, it was assumed that the crack would be located exactly below the middle of the loads the train would exert on the rail. As the loads are the highest here, this point was taken. In reality, it could be the case that an existing crack is not situated exactly below the train wheel. In that case the stresses in the rail could be different, such that the SIFs in the cack tips get different results. This could have a significant influence on the Damage Index and is thus something that should be taken into consideration. With this model, it has not been analysed how the SIFs or the Damage Index would change by moving the crack away from the middle of the load.

Then there are some discussion points regarding the obtained results. By analysing the parameter influence on the WLRM, it was found that the vertical wear depth has a significant influence on the Damage Index. This influence is not simply linearly described. At least a quadratic formulation is needed, if not higher orders, to describe the influence of the vertical wear depth. Further research would be needed to give more insight into the influence of this parameter.

A large discussion point is the real added value of the WLRM. As has been shown, it is difficult to draw an RCF curve for specific cases. It could be possible that the inclusion of the initiation phase, as well as the changing crack growth, improves the results. Nevertheless, even if the WLRM could be drawn, the added value could be discussed. For specific cases, the Damage Index and wear number could easily be obtained for RCF as well as for wear. As has been shown, the dominant failure mechanism can be found and a prediction of the number of cycles until failure can be defined. By constructing the full WLRM for a specific case, the lines would only show the already found Damage Indices and a graph which is not necessarily useful for any other case. Even though the idea of the WLRM is useful, it can be argued that the full graph is obsolete.

In the end, the reason for writing this study has been discussed. In the unpublished work of Meghoe et al. [2], a model was set up to predict the Damage using wear and RCF. The reviewfailure mechanism can be found and er of this paper had certain difficulties with this model, which proved to be enough to reject the paper. These difficulties were mainly formed by the RCF part of the model. It was too much dependent on elastic material parameters, only a limited range of contact conditions was analysed and there where some wheel-rail contact assumptions made which were not fully valid. Because of these points, this study was set up to find another way in which the crack growth in rails could be predicted. In this study it was tried to use FEM models to predict the crack growth. LEFM is still used as the basis for the model as multiple other researches use similar approaches [40, 45]. Nevertheless, a FEM model is used that describes the stresses in the crack locally. This will give increased significance in the possible stress calculation. Next to the different model, The contact conditions have been analysed by looking at different parameters for the contact conditions. Different radii, cant, and speeds have been used to simulate rail contact. In that, also the friction for different friction coefficients is taken into consideration. The vertical wear depth was also used as input parameter to be included into the analysis. The part still missing to fill this gap completely is the addition of looking at different rail material grades, different geometries and different wheel geometries. The tonicity of the wheels could have different effects on the stresses in the crack, but these geometries have not been researched yet.

5 | Conclusion and Recommendation

5.1 Conclusion

In this study, it was tried to find a possible approach to construct the RCF function of a WLRM. This study aimed to find an approach that could be used to construct the RCF part of the WLRM, by using operational data as input values. To set up such an approach, the crack growth on rails was studied and divided into an initiation phase and a propagation phase. Both phases need their own prediction model to get a full view of the RCF crack growth. Due to time constraints, this study only included the propagation phase. From the literature review, it was found that a FEM model would be a preferable method to model crack propagation in rails. An extended finite element method (XFEM) was chosen as this method makes the analysis of propagating cracks easier and requires less computational effort. Using this model, the Burstow WLRM RCF part was recreated, the influence of different input parameters was analysed and a test case was set up to see if it could be used on real cases. From this study, the following conclusions have been drawn:

- Using the framework from Figure 3.6 it is possible to determine the wear number and Damage Index for a specific case

- If loads and frictions comparable to Burstow's field results are used, Damage Indices within a range of the existing WLRM of Burstow can be found. The RCF part of the WLRM can be obtained by these points

- From the eight analysed parameters, the vertical wear depth, axle load, train speed and coefficient of friction have a significant influence on the RCF function. For the other parameters, the influence is less significant. The longitudinal and lateral stiffness can be neglected due to their low influence.

- For a theoretical case it is still difficult if not impossible to derive the RCF function. Due to the significant and complex influence of some operational parameters on the Damage Index, no straight line can be found. The Damage Indices create a cloud in the WLRM from which no RCF curve can be drawn. For real cases, the same is expected

- It is possible to find the dominant failure mechanism (wear/RCF) for a case and determine in which phase of the WLRM a specific case is placed.

From the conclusions drawn, it can be seen that the aim of this study has not fully been achieved yet. A method has been developed to obtain the RCF function, but it has been proven that obtaining the RCF function is more difficult and requires more research.

5.2   Recommendation

As a closure, some recommendations have been made which are needed for further development of the RCF model. A number of important developments have already been discussed that require further research. Some aspects of crack formation have been neglected in this study but should still be implemented in a prediction method like the WLRM. In the list below, a number of these developments is given;

- The crack initiation model should be included into the prediction model. Important for such a model is the location where the crack will start to grow as well as the threshold stresses needed to initiate the crack. Expected is that the initiation will give more insight into the threshold value of the RCF function and its place in the WLRM.

- Changing crack growth due to changing crack size should be included into the Damage Index calculation. As the crack size and thus the growth rate is dependent on time and the number of cycles passed, it is suggested to add a certain timescale. This would show the growth rate and crack size after a certain amount of cycles, which would better indicate the state of the rail.

- In the parameter influences, it is seen that the vertical wear depth has significant influence, but its behaviour is not simply linear. It is beneficial to do further research into this behaviour, as the wear depth is not described linearly or quadratically, but otherwise.

- Instead of the used UIC-54 geometry with R260 steel, other rail geometries and steel grades should be tested to see if different results are obtained. Expected is that a geometry change would not be very significant other than a possible change in crack location. The steel grade will be influential because material properties such as the Young's Modulus and the Poisson ratio are of importance in the SIF calculations.

- In the same category, also the wheel profiles of the crossing trains should be varied. The study only uses one wheel, while different geometries and materials can be used for that as well. Expected is a different stress field running over the model and thus different stresses and SIFs in the crack.

- The crack geometry and location should be varied. As has been shown, the geometry of the crack influences the growth rate. Because cracks are not expected to grow as simple elliptical cracks, a way to include this in the growth rate calculations has to be found.

- Finally, the idea of the WLRM should be tested on real-life cases. With an experimental test, it could be validated if the WLRM is describing the crack formation properly. Labaratory tests could be performed to validate the if the crack growth predicts similar to the way the WLRM predicts this growth. In the end, the useability on real life rail maintenance should be tested.

References

[1] M. Burstow. Whole life rail model application and development for rssb - development of an rcf damage parameter. Report, Rail Safety and Standards Board, 2003.

[2] Annemieke Meghoe, Richard Loendersloot, and Tiedo Tinga. Generic rail damage function based on physical models. Unpublished manuscript, 2020.

[3] R.P.B.J. Dollevoet. *Design of an anti head check profile based on stress relief.* Thesis, University of Twente, 2010.

[4] Mark Burstow. Management and understanding of rolling contact fatigue: Wp1 mechanisms of crack initiation, final report. Report, Rail Safety and Standards Board, 2008.

[5] Mark Burstow. Vtac calculator: Guidance note for determining $t\gamma$ values. *Network Rail*, 2012.

[6] Martin Hiensch and Michaël Steenbergen. Rolling contact fatigue on premium rail grades: Damage function development from field data. *Wear*, 394-395:187–194, 2018. ISSN 0043-1648. doi: 10.1016/j.wear.2017.10.018.

[7] Q. Wang. Effect of inclusion on subsurface crack initiation and gigacycle fatigue strength. *International Journal of Fatigue*, 24(12):1269, 2002. ISSN 0142-1123 0142-1123.

[8] C. Marte, G. Trummer, A. Aichmayr, P. Dietmaier, and K. Six. Sensitivity analysis: Main parameters causing wear and rolling contact fatigue in wheel-rail contact. *The Dynamics of Vehicles on Roads and Tracks*, page 1179, 2016. ISSN 9780429094729.

[9] J. Schijve. Fatigue of stuctures and materials, 2009.

[10] Dimitris Chrysafopoulos. Stress intensity factors for fatigue crack growth analysis, 2014.

[11] Bob McGinty. Stress intensity factor, 2014. URL https://www.fracturemechanics.org/sif.html.

[12] Michael Janssen, Jan Zuidema, and Russell Wanhill. *Fracture Mechanics: An Engineering Primer*. TU Delft OPEN, 2024. ISBN 978-94-6366-818-7. doi: https://doi.org/10.59490/tb.86.

[13] Q. Jane Wang and Yip-Wah Chung. Encyclopedia of tribology, 2013.

[14] Olga Ivankova Matús Turis. Using finite element analysis to obtain plastic zones in the vicinity of the crack edges, under mixed mode loading conditions. *MATEC Web of Conferences*, 310, 2020. doi: https://doi.org/10.1051/matecconf/202031000028.

[15] F. Erdogan P.C. Paris. A critical analysis of crack propagation laws. *Journal of Basic Engineering*, 85:528–533, 1963. doi: http://dx.doi.org/10.1115/1.3656900.

[16] K. Rege and H. G. Lemu. A review of fatigue crack propagation modelling techniques using fem and xfem. *IOP Conference Series: Materials Science and Engineering*, 276:012027, 2017. ISSN 1757-8981. doi: 10.1088/1757-899x/276/1/012027.

[17] M. J. Mullins. Mechanical properties of thermosets. *Thermosets*, page 28, 2012. ISSN 9780857090867.

[18] Qiang Bai. Fatigue and fracture. *Subsea Pipeline Design, Analysis, and Installation*, page 283, 2014. ISSN 9780123868886.

[19] S. Meyer, A. Brückner-Foit, and A. Möslang. A stochastic simulation model for microcrack initiation in a martensitic steel. *Computational Material science*, 26: 102–110, 2003. doi: https://doi.org/10.1016/S0927-0256(02)00409-3.

[20] M. Goto. Statistical investigations of the behaviour of microcracks in carbon steels. *Fatigue and Fracture of Engineering Materials and Structures*, 14:833–845, 1991. doi: https://doi.org/10.1111/j.1460-2695.1991.tb00715.x.

[21] C. Ihara and T. Tanaka. A stochastic damage accumulation model for crack initiation in high-cycle fatigue. *Fatigue and Fracture of Engineering Materials and Structures*, 25:375–380, 2001. doi: https://doi.org/10.1046/j.1460-2695.2000.00308.x.

[22] V. Krishna. *Long freight trains and long-term rail surface damage*. PhD thesis, KTH Royal Institute of Technology, 2022.

[23] Visakh V. Krishna, Saeed Hossein-Nia, Carlos Casanueva, Sebastian Stichel, Gerald Trummer, and Klaus Six. Rail rcf damage quantification and comparison for different damage models. *Railway Engineering Science*, 30(1):23–40, 2022. ISSN 2662-4753. doi: 10.1007/s40534-021-00253-y.

[24] A. Ekberg, B. Åkesson, and E. Kabo. Wheel/rail rolling contact fatigue probe, predict, prevent. *Wear*, 314(1-2):2, 2014. ISSN 0043-1648 0043-1648.

[25] B. Dirks, R. Enblom, A. Ekberg, and M. Berg. The development of a crack propagation model for railway wheels and rails. *Fatigue and Fracture of Engineering Materials and Structures*, 38(12):1478–1491, 2015. ISSN 8756-758X. doi: https://doi.org/10.1111/ffe.12318.

[26] F. Franklin, I. Widiyarta, and A. Kapoor. Computer simulation of wear and rolling contact fatigue. *Wear*, 251(1-12):949, 2001. ISSN 0043-1648 0043-1648.

[27] G. Trummer and et al. Modeling surface rolling contact fatigue crack initiation taking severe plastic shear deformation into account. *Wear*, 352-353:136–145, 2016. ISSN 0043-1648 0043-1648.

[28] H.-P. Gänser J. Maierhofer, R. Pippan. Modified nasgro equation for physically short cracks. *International Journal of Fatigue*, 59:200–207, 2014.

[29] S. A. Kanth, G. Harmain, and A. Jameel. Modeling of nonlinear crack growth in steel and aluminum alloys by the element free galerkin method. *Materials Today: Proceedings*, 5(9):18805, 2018. ISSN 2214-7853 2214-7853.

[30] Stanislaw Bogdański, Jacek Stupnicki, Mike W. Brown, and Dawid F. Cannon. *A Two Dimensional Analysis of Mixed-Mode Rolling Contact Fatigue Crack Growth in Rails*, pages 235–248. Elsevier, 1999. ISBN 1566-1369. doi: 10.1016/s1566-1369(99)80018-1.

[31] Reza Masoudi Nejad, Khalil Farhangdoost, and Mahmoud Shariati. Three-dimensional simulation of rolling contact fatigue crack growth in uic60 rails. *Tribology Transactions*, 59(6):1059–1069, 2016. ISSN 1040-2004. doi: 10.1080/10402004.2015.1134738.

[32] R. Masoudi Nejad, M. Shariati, and K. Farhangdoost. Effect of wear on rolling contact fatigue crack growth in rails. *Tribology International*, 94:118, 2016. ISSN 0301-679X 0301-679X.

[33] R. Branco, F. Antunes, and J. Costa. A review on 3d-fe adaptive remeshing techniques for crack growth modelling. *Engineering Fracture Mechanics*, 141:170, 2015. ISSN 0013-7944 0013-7944.

[34] A. M. Alshoaibi and Y. A. Fageehi. 2d finite element simulation of mixed mode fatigue crack propagation for cts specimen. *Journal of Materials Research and Technology*, 9(4):7850, 2020. ISSN 2238-7854 2238-7854.

[35] Abdulnaser M. Alshoaibi and Yahya Ali Fageehi. Simulation of quasi-static crack propagation by adaptive finite element method. *Metals*, 11(1), 2021. doi: https://doi.org/10.3390/met11010098.

[36] J. R. Rice. A path independent integral and the approximate analysis of strain concentration by notches and cracks. *Journal of Applied Mechanics*, 35(2):379, 1968. ISSN 0021-8936.

[37] C. F. Shih, B. Moran, and T. Nakamura. Energy release rate along a three-dimensional crack front in a thermally stressed body. *International Journal of Fracture*, 30(2):79–102, 1986. ISSN 0376-9429. doi: 10.1007/bf00034019.

[38] J. F. Yau, S. S. Wang, and H. T. Corten. A mixed-mode crack analysis of isotropic solids using conservation laws of elasticity. *Journal of Applied Mechanics*, 47(2): 335, 1980. ISSN 0021-8936.

[39] *Abaqus User Manual; The extended finite element method (XFEM)*. Dassault Systèmes Simulia Corp., 2016.

[40] B. Rodríguez-Arana and et al. Xfem rolling contact fatigue crack propagation in railways considering creepages on contact shear stresses. *Engineering Fracture Mechanics*, 276:108896, 2022. ISSN 0013-7944 0013-7944.

[41] D. Bóbis and P. T. Zwierczyk. Introduction of a possible approach to modelling the propagation of head check cracks using the extended finite element method taking into account fluid penetration. In *Proceedings - European Council for Modelling and Simulation, ECMS*, volume 37, pages 131–137, 2023. Export Date: 21 December 2023; Cited By: 0.

[42] D. Bóbis, P. T. Zwierczyk, and T. Máté. Application of the extended finite element method in the aim of examination of crack propagation in railway rails. In *Proceedings - European Council for Modelling and Simulation, ECMS*, volume 36, pages 210–216, 2022. Export Date: 21 December 2023; Cited By: 1.

[43] *Abaqus User Manual; Modeling discontinuities as an enriched feature using the extended finite element method*. Dassault Systèmes Simulia Corp., 2016.

[44] E. Ferro, J. Harkness, and L. Le Pen. The influence of sleeper material characteristics on railway track behaviour: concrete vs composite sleeper. *Transportation Geotechnics*, 23, 2020. doi: https://doi.org/10.1016/j.trgeo.2020.100348.

[45] S.H. Mai, A. Gravouil, M.L. Ngyuyen-Tajan, and B. Trollé. Numerical simulation of rolling contact fatigue crack growth in rails with the rail bending and the frictional contact. *Engineering Fracture Mechanics*, 174:196–206, 2017. doi: https://doi.org/10.1016/j.engfracmech.2016.12.019.

[46] M.S. Sichani. *On Efficient Modelling of Wheel-Rail Contact in Vehicle Dynamics Simulation*. PhD thesis, KTH Royal Institute of Stockholm, 2016.

[47] J.J. Kalker. *On the rolling contact of two elastic bodies in the presence of dry friction*. PhD thesis, TU Delft, 1967.

[48] J.J. Kalker. Rolling contact phenomena: Linear elasticity. Technical report, TU Delft, 2000.

[49] *Simulia User Assistance 2020*. Dassault Systèmes SE., 2020.

[50] *Abaqus User Manual; Stress intensity factor extraction*. Dassault Systèmes Simulia Corp., 2006.

[51] P.E. Bold, M.W. Brown, and R.J. Allen. Shear mode crack growth and rolling contact fatigue. *Wear*, 144:307–317, 1991. doi: https://doi.org/10.1016/0043-1648(91)90022-M.

[52] S. Bogdanski, J. Stupnicki, M.W. Brown, and D.F. Cannon. A two dimensional analysis of mixed-mode rolling contact fatigue crack growth in rails. *European Structural Integrity Society*, 25:235–248, 1999. doi: https://doi.org/10.1016/S1566-1369(99)80018-1.

[53] A. Meghoe, R. Loendersloot, and T. Tinga. Rail wear and remaining life prediction using meta-models. *International Journal of Railway Transportation*, 8:1–26, 2019. doi: https://doi.org/10.1080/23248378.2019.1621780.

[54] T.M. Cioppa and T.W. Lucas. Efficient nearly orthogonal and space-filling latin hypercubes. *Technometries*, 49:45–55, 2007.

[55] J. Dong, W. Pei, H. Ji, H. Long, X. Fu, and H. Duan. Fatigue crack propagation experiment and numerical simulation of 42crmo steel. *Journal of Mechanical Engineering Science*, 234:1–11, 2020. doi: http://dx.doi.org/10.1177/0954406220910458.

[56] B. Trollé, M.C. Baietto, A. Gravouil, S.H. Mai, and T.M.L. Nguyen-Tajan. Xfem crack propagation under rolling contact fatigue. *Procedia Engineering*, 66:775–782, 2013. doi: http://dx.doi.org/10.1016/j.proeng.2013.12.131.

[57] D. Sung, S. Hong, and J. Lee. Numerical analysis of the rail surface crack propagation under rail uplift force: A parametric study on initial crack geometry. *Engineering Failure Analysis*, 153, 2023. doi: https://doi.org/10.1016/j.engfailanal.2023.107542.

A | Burstow Results

A.1 Burstow WLRM

In his work, Burstow [4] defined the WLRM by looking at three different locations and drawing a line through the obtained points. Figure A.1 shows this obtained model. To obtain these points, he studied three locations with multiple different train types and wheel geometries running at these locations. For the Leigh-on-Sea location, the main force and contact patch parameters are given. These are shown in Figure A.2. The ranges of these parameters are used to determine the load parameters from Table 3.3. Finally Figure A.3 shows the crack growth of multiple cracks in the Harringay location. As can be seen, the cracks mainly start to grow linearly after 0.003 m of length has been reached.
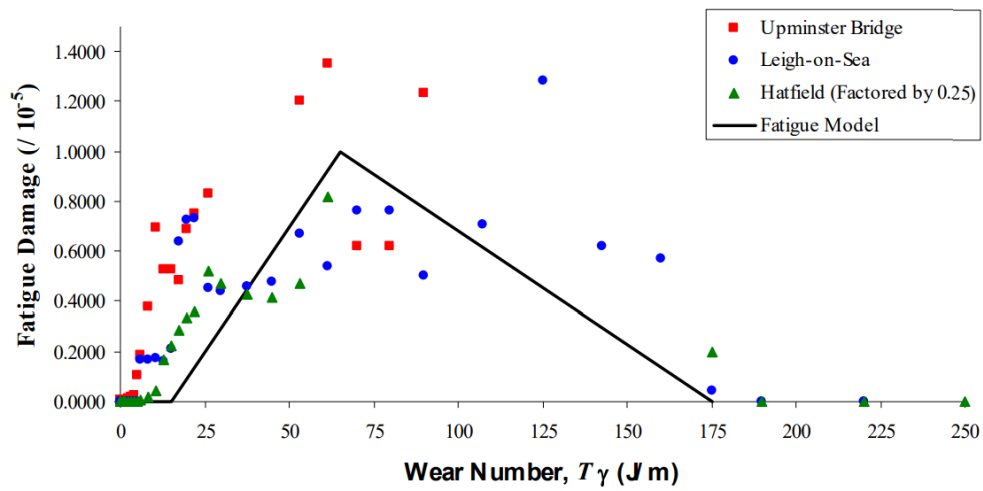

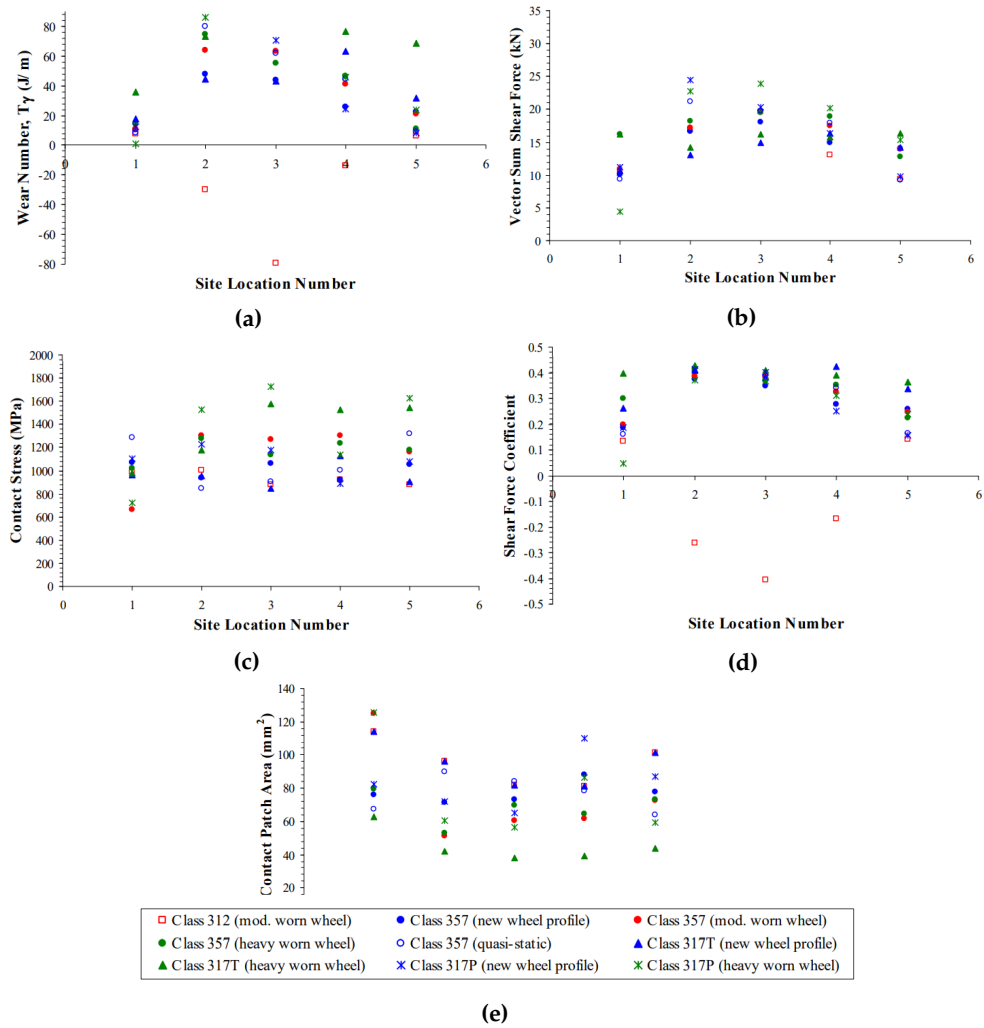**Figure A.1:** *The WLRM obtained by Burstow, including data points from field results*
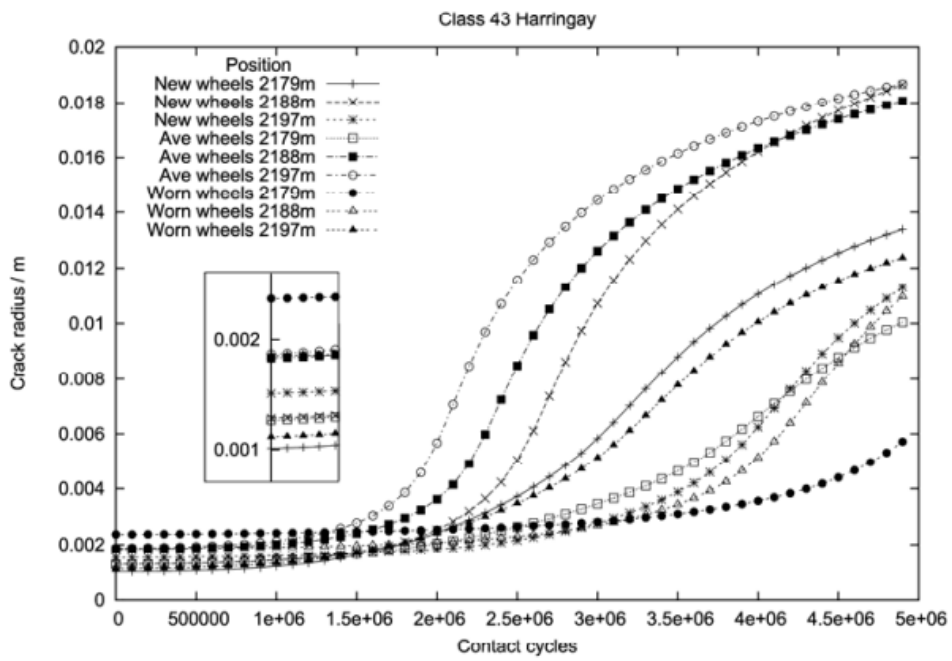
Figure A.2: *Load parameters for Leigh-on-Sea case Burstow*

Figure A.3: *Crack size after a certain amount of cycles*